INVESTIGATION OF ELASTIC SCATTERING CROSS-SECTION DEPENDENCE ON TARGET MASS NUMBER USING SCAT2

PhD DISSERTATION

THU ZAR YIN

DEPARTMENT OF PHYSICS
UNIVERSITY OF YANGON
MYANMAR

APRIL 2005

INVESTIGATION OF ELASTIC SCATTERING CROSS-SECTION DEPENDENCE ON TARGET MASS NUMBER USING SCAT2

THU ZAR YIN

THIS DISSERTATION IS SUBMITTED TO THE BOARD OF EXAMINERS IN PHYSICS, UNIVERSITY OF YANGON FOR THE DEGREE OF DOCTOR OF PHILOSOPHY

Tin Aung

EXTERNAL EXAMINER

Professor Dr Tin Aung
HOD Physics (Rtd)
University of Yangon

Sein Htoon

CHAIRMAN

Professor Dr Sein Htoon
CSci CPhys FInstP (Lond)
Head of Department of Physics & IT
Yangon University

Devendra Mohan

EXTERNAL EXAMINER

Professor Dr Devendra Mohan
Department of Quantum Electronics
Guru Jambheshwar University, India

May

EXTERNAL EXAMINER

DR MAY MYINT SI
M Sc, PhD
Professor in Physics
Department of physics
Hinthada University

SUPERVISOR

Dr. Win Sin
MSc, PhD (Ygn), HGP
Assistant Lecturer in Physics
University of Yangon.

CONTENTS

ACKNOWLEDGEMENTS

I would like to express my profound thanks to Professor Dr Sein Htoon, PhD *Sur* CSci CPhys FInstP *Lond*, Head of Department of Physics (IT), Dean of Engineering, Director of IAEA Nuclear Physics Lab, University of Yangon, for his kind permission to carry out this work and his encouragement and help during this work.

My sincere thanks also go to my supervisor Dr Win Sin, PhD, Assistant Lecturer in Physics & IT, Yangon University, for his guidance and help throughout this work.

It is my pleasure to express my sincere thanks to all members of the staff and Computing Assistants of Department of Physics (IT), University of Yangon, for their constant encouragement and help during this research work.

Abstract

Theoretical studies of systematics of neutron scattering cross sections on various materials for neutron energies up to several MeV are of practical importance. In this work, we investigate Elastic Cross-section Dependence on Target Mass Number using Statistical Optical Model code SCAT2. We also compare the calculated cross-sections with those given in Evaluated Nuclear Data File (ENDF-VI).

CHAPTER 1
INTRODUCTION

In its broadest sense, the subject of nuclear reactions includes all those processes in which a nucleus interacts with another nucleus or an elementary particle. When we study these processes, we want to understand what happens, and this means understanding the probabilities for the emission of various particles, their polarizations and correlations, indeed all the features of the reaction that can be experimentally determined. By "understand" we mean not only the ability to calculate these probabilities from theories of nuclear reactions and nuclear structure, but also the physical understanding that enables us to know, to some extent, what will happen in particular cases even before we make any calculations.

The process of understanding proceeds in several interacting stages. Firstly come the experimental data on reactions, itself often obtained in response to previous theoretical speculations. Secondly there is the idea that perhaps this data may be understood by using a particular model of the nucleus concerned. Thirdly this model is expressed in mathematical form, developed to account for the reaction of interest, programmed for a computer, and used to obtain quantitative predictions. Fourthly these predictions are compared with the data, and conclusions drawn about the applicability of the model. These may suggest more experiments, the modification of the model used, or the development of a new model.

Over the last seventy years, many studies of the nuclear reactions have been made, and a vast amount of data accumulated. Much of this is quite well understood in terms of nuclear reaction and nuclear structure theories.

In recent times, the concept of an accelerator driven subcritical (ADS) system is drawing worldwide attention. In this ADS system, neutrons are produced by bombarding a heavy element target with a high energy proton beam of typically above 1.0 GeV with a current of greater than 10 mA. Such a system serves a dual purpose of energy multiplication and waste incineration. In this context, theoretical study of systematic of neutron scattering cross-sections on various materials for neutrons energies up to several hundred MeV are of practical importance.

Nuclear cross-section data are needed for many applications in science and technology. Mostly these cross-section data are supplied by experiment. There are, however many situations where model calculations can supply experimental cross-sections. Using "ABAREX", "SCAT2", "ALICE" ...etc, we can calculate the integrated and differential cross-sections for a particular target with incident particle of different energies.

In this work we investigate the elastic cross-section dependence on target mass number using SCAT2 especially for 3-Li-7, 6-C-12, 12-Mg-24, 17-Cl-36, 20-Ca-40, 22-Ti-48, 26-Fe-56, 30-Zn-64, 32-Ge-72, 38-Sr-84, 42-Mo-96, 48-Cd-108, 50-Sn-120, 54-Xe-132, 60-Nd-144, 64-Gd-160, 72-Hf-180, 81-Tl-200, 90-Th-232 and 92-U-238, using SCAT2 and compare the results with those given in ENDF VI. We chose the targets to be light ones, intermediates ones and heavy ones so that the code may be valid for all kinds of nuclides. We see the results are quite the same and SCAT2 is found to be an efficient tool in studying nuclear cross-sections.

CHAPTER 2

THE IDEA OF OPTICAL MODEL

2.1 Introduction

When a projectile undergoes elastic scattering, the internal energy of the target is unchanged but the projectile is scattered out of the incident beam in a manner which depends on the interaction between the projectile and the target.

Since the nucleus is a quantized system it may exist in one of a discrete spectrum of excited states, each one characterized by a set of quantum numbers, and the higher states may be excited in the process of inelastic scattering in which the projectile transfers a definite amount of energy to the nucleus. Alternatively, the projectile may be captured and a different particle may be emitted, or the original particle may reappear accompanied by other particles. In each of these processes the residual nucleus is left in a well-defined state [11].

Thus the study of elastic scattering provides information about the nucleus in its normal or ground state, while the study of inelastic scattering and reactions provides information on the existence, location and properties of its excited states. Each process is characterized by a cross-section σ which may be defined as the probability that the process will occur if the incident beam carries one particle per second and the target contains one nucleus per unit area.

The cross-section $d\sigma$ measures the probability that the reaction product will appear within a solid angle $d\Omega$ about a given direction. The angular distribution of the reaction product as a function of the scattering angle is normally measured at a fixed energy corresponding to one of the peaks in the energy spectrum. This measurement gives the differential cross-section $d\sigma/d\Omega$ for the excitation of a particular final state.

Some information can be deduced directly from the appearance of the various cross-sections but more detailed interpretation requires a comparison with theoretical predictions for the cross-section. The interaction V(r) between the projectile and the target is a function of their relative positions, i.e. $\mathbf{r} = \mathbf{r}_1 - \mathbf{r}_2$, and it is therefore convenient to transform from the laboratory frame of reference in which the target is

at rest before collision to the center-of-mass frame in which the centre-of-mass of the whole system is permanently at rest [8].

The same general result holds in quantum mechanics and we have to solve the Schrödinger equation for the particle of reduced mass for a suitably chosen interaction potential and to obtain particular solutions by applying the appropriate boundary conditions.

In the laboratory frame, the incident beam passes through a collimating slit before reaching the target and so forms a wave packet but the size of the wave packet is so large compared with the size of region in which the scattering potential is effective that it is a good approximation to replace the wave packet by a plane wave of infinite extent.

In the centre-of-mass frame, the time-dependent wavefunction is given by

$$\Psi = \psi e^{-iE_t/\hbar} \tag{2.1}$$

and time-dependent equation is

$$\nabla^2\psi + \frac{2\mu}{\hbar^2}[E - V]\psi = 0 \tag{2.2}$$

Before the scattering occurs we have a collimated beam of particles moving along the z-direction with momentum $\hbar k = \mu v$. This beam is represented by the plane wavefunction

$\psi = e^{ikz}$ which is the solution of equation (2.2) with V= 0.

For the incident beam the probability density is

$$P_{in} = \psi^* \psi = 1 \tag{2.3}$$

and the probability current density is

$$j_{in} = \frac{\hbar}{2\mu i}(\psi^* \nabla\psi - \psi \nabla\psi^*) = \frac{\hbar k}{\mu} \tag{2.4}$$

If the beam is scattered by a spherically symmetric potential V(r) the scattered wave must have the form at large distances from the potential of an outgoing spherical wave with axial symmetry.

The wavefunction of such a scattered wave is $(e^{ik'r}/r)f(\theta)$ where $f(\theta)$ is some function of the scattering angle θ which depends on the exact form of the potential.

For the scattered beam the probability density is

$$P_{out} = \frac{|f(\theta)|^2}{r^2} \tag{2.5}$$

and the probability current density is

$$j_{out} = \frac{\hbar k'}{\mu r^2}|f(\theta)|^2 \tag{2.6}$$

On the surface of a sphere the element of area is $ds = r^2\, d\Omega$, so that the current passing through an element of solid angle $d\Omega$ is $(\hbar k'/\mu)|f(\theta)|^2 d\Omega$, but the cross-section $d\sigma$ is just the ratio of the flux through the solid angle $d\Omega$ to the incident flux. Hence

$$d\sigma = \frac{k'}{k}|f(\theta)|^2 d\Omega \tag{2.7}$$

and for elastic scattering $k' = k$ so that

$$\frac{d\sigma}{d\Omega} = |f(\theta)|^2 \ . \tag{2.8}$$

To calculate the cross-section we have to solve the time-dependent Schrödinger equation with a given potential and find a solution ψ which has the asymptotic behaviour of an outgoing scattered wave and an incoming plane wave, i.e.

$$\psi \xrightarrow[r\to\infty]{} e^{ikz} + f(\theta)\frac{e^{ik'r}}{r} \tag{2.9}$$

The differential cross-section in the laboratory system is related to the differential cross-section in the centre-of-mass system by the expression

$$\frac{d\sigma}{d\Omega}(\theta_{lab}) = \frac{(1+\nu^2+2\nu\cos\theta)^{3/2}}{|1+\nu\cos\theta|}\ \frac{d\sigma}{d\Omega}(\theta) \qquad (2.10)$$

Where ν is the ratio of the speed of the centre-of-mass in the laboratory system to the speed of the scattered particle in the centre-of-mass system, and

$$\tan\theta_{lab} = \sin\theta/(\nu+\cos\theta)\ . \qquad (2.11)$$

The total cross-section is given by

$$\sigma = 2\pi\int_0^{\pi}\frac{d\sigma}{d\Omega}\sin\theta\, d\theta\ . \qquad (2.12)$$

The interaction between the nucleon and the nucleus can be represented by a potential which varies smoothly with mass number A and projectile energy E, and a residual interaction. Scattering due to the potential is called shape elastic or potential scattering.

When the incident nucleon interacts with the nucleons in the nucleus through the residual interaction the target nucleus becomes excited. If the nucleon has moderately high energy, the major part of this energy is quickly carried away of an emitted particle, and a direct reaction or direct inelastic scattering occurs. If the incident nucleon makes repeated interactions inside the nucleus, the structure of the (A+1) system becomes very complicated and the energy of the incident nucleon becomes distributed among many particles. At this point it is said that a compound nucleus has been formed, and examination of the cross-section as a function of the energy of the incident nucleons shows sharp peaks or resonances which correspond to the formation of a quantized state of the (A+1) system.

Eventually the compound nucleus must decay and the incident nucleon may reappear to give compound elastic scattering. The occurrence of the various non-elastic processes means that nucleons are lost from the incident beam and hence the number of nucleons in the elastically scattered beam is reduced. This effect is taken into account in calculations by including in the potential a part which causes a reduction in the intensity of the scattered beam, and this total potential which describes the elastic scattering is called the optical potential.

2.2 The Optical Model

In the study of nuclear reactions the concept of the compound nucleus (the statistical model for nuclear reactions) is not always reliable. The statistical nature of the compound nucleus theory implies that its predictions are at best averages, and do not take into account the differences between specific nuclei. Therefore a more detailed model is needed for the description of nuclear reactions.

The statistical model assumes that the compound nucleus is formed immediately when the incident neutron reaches the nuclear surface. The cross-section for reaching the surface turns out to be a monotonically decreasing function of the energy, varying as $E^{-1/2}$ for small energies and reaching the asymptotic value $2\pi R^2$ for large energies. At the neutron energies involved, between 0.1 MeV and several MeV, and for intermediate or heavy nuclei, individual resonances cannot be resolved, and the measured cross sections are averages over many levels.

The optical model describes the effect of the nucleus on the incident particle by a potential well $-V_0$ (r), but allows for the possibility of compound nucleus formation by adding to the potential a negative imaginary part, $-iV_1(r)$. This part produces absorption of the incident particle within the nucleus, and this absorption is supposed to represent the formation of the compound nucleus [1].

The basic task of nuclear-reaction theory is to find a solution of the Schrödinger equation of the system under consideration that satisfies the appropriate boundary conditions. This Schrödinger equation is a many - particle one, so that the total wave function depends on the coordinates of all the interacting particles, and the potential is the sum of all the interactions between them. To solve such an equation is an almost impossible task, so at the outset we assume that the interaction between the incident particle and the target nucleus can be represented by a simple one-body potential V(r), where r is their separation. This assumption may be partly justified by considering the single-particle shell model, and the general form of V(r) can be found. Throughout the analysis we work in the centre – of – mass system, with the exception that by convention the energy of the incident particle is quoted in the laboratory system.

On the optical model, compound nucleus formation does not occur immediately or with complete certainty. Even if the incident particle has entered the nucleus, it is removed from its free particle state only with some delay and with a certain probability. The model has also been extended and applied with more complicated potential functions to other nuclear reactions and cross sections.

The feature of nuclear scattering cross sections can be explained by a very simple model in which we represent the interaction between the incident nucleons and the nucleus by a one-body potential that depends only on the nuclear radius. This is called the optical model.

2.3 Nuclear Scattering Processes and Optical Model Potential

The optical model potential can be used to calculate the differential cross-section for the elastic scattering of nucleons by nuclei making use of the quantum mechanical scattering formalism. This calculation gives only the direct elastic scattering so the comparison with the experimental cross-section must only be made at energies high enough for the compound elastic cross-section to be negligible [2].

The potential experienced by a particle incident on a nucleus is the extension to positive energies of the shell-model potential for bound nucleons. The full optical potential is

$$V(r) = V_c(r) + U f_u(r) + i w f_u(r) + V_{so}(r) \qquad (2.13)$$

$$V_c(r) = \frac{Z_I Z_T e^2}{2Rc}\left(3 - \frac{l^2}{R_c^2}\right), \qquad r < R_c \qquad (2.14)$$

$$V_c(r) = \frac{Z_I Z_T e^2}{r}, \qquad r > R_c \qquad (2.15)$$

where Z_I and Z_T are the charges of the incident particle and target nucleus.

The Coulomb potential $V_c(r)$ is that of a charged particle in the electrostatic field of the nucleus. This is calculable from the nuclear charge distribution, but in practice it is sufficiently accurate to use the potential due to a sphere of radius R_c with its charge uniformly spread throughout its volume.

The real part of the potential is due to the action of all the nucleons in the nucleus on the incident particle, and is thus approximately given by

$$U(r) = \sum_i V(|r - r_i|) \approx \int \rho(r')\ V(|r - r'|)dr' \qquad (2.16)$$

where $\rho(r')$ is the nuclear density and $V|r - r'|$ the effective interaction between the incident particle and a nucleon in the nucleus. Since the nucleon-nucleon interaction has short range, it can be expressed by a delta function, giving ,

$$V(r) \approx \int \rho(r') V_0\, \delta(r - r')dr' = U_0\, \rho(r) \qquad (2.17)$$

Thus to first approximation we expect the optical potential to have a radial variation that follows the nuclear density quite closely, with perhaps a somewhat greater radius reflecting the finite range of the nucleon-nucleon interaction. It is useful to represent this radial dependence by an appropriate analytical expression, and for this purpose the Saxon-Woods form is particularly convenient so the real potential becomes

$$U(r) = U\, f_u(r) = \frac{u}{1 + \exp(\frac{r - R}{a})} \qquad (2.18)$$

where R is the radius and a is the surface diffuseness parameter.

The nucleon-nucleon interaction is purely real, so this argument applies only to the real part of the nucleon optical potential. Feshbach, Porter and Weisskop assumed that the real and imaginary parts of the optical potential have the same form, and this is still widely followed. Since the imaginary potential takes into account in a global way all the non-elastic processes that remove flux from the elastic channel it is not possible to establish its form by simple physical arguments. The best fits are obtained by adding to the volume imaginary potential a surface-peaked potential of the radial derivative form.

$$g(r) = -4a\frac{df(r)}{dr} = \frac{4\exp(\frac{r - R}{a})}{[1 + \exp(\frac{r - R}{a})]^2} \qquad (2.19)$$

where the factor 4a is introduced to ensure that g (R) = 1.

The imaginary part of the potential increases in magnitude with the energy to take account of the increasing cross-sections of the various non-elastic reactions.

These radial forms for the nucleon optical potential sufficed until quite recently, when evidence from proton elastic scattering indicated the need for a modified form at higher energies.

Nucleons have spin one-half, and even if the incident beam is unpolarised we find that the scattered beam is polarised. This polarisation can be calculated from the optical model which is added spin-dependent term [3].

The spin orbit term is

$$V_{so}(r) = (\frac{\hbar}{mc})^2 \; Vs \; \frac{1}{r} \; \frac{df_s(r)}{dr} \; L\sigma \qquad (2.20)$$

The form factor $f_s(r)$ has the Saxon-Woods analytical and usually a rather smaller value of the radius parameter. This spin orbit potential is the extension to positive energies of the term in the simple shell model potential that gives the spin-orbit splitting needed to account for the magic numbers.

With the addition of the spin-orbit term to the optical model potential the calculation of the observable quantities from the Schrödinger equation proceeds in essentially the same way as before, except that now there are two radial wave equations corresponding to the two possible spin orientations relative to the orbital angular momentum. These combine vectorially, J=L+S so that $J = L \pm \frac{1}{2}$. The phase shifts corresponding to these two spin orientations for each L can be combined to give not only the differential cross-section but also the polarization as a function of the scattering angle.

The optical model can be applied to the scattering of deuterons, tritons, alpha-particles and heavier nuclei. Many optical model analyses have been made of the elastic scattering of deuterons, hellions, tritons and alpha-particles by nuclei. As for nucleons, the depths of the real and imaginary parts of the potential, and of the spin-

dependent terms are found to vary smoothly with energy and from one nucleus to another.

There are many other processes that can take place in the time it takes the projectile to cross the target nucleus. The simplest is inelastic scattering, which gives energy to the target, raising it to an excited state. The projectile emerges with reduced energy and changed state of polarization. Such processes generally excite the collective states of nuclei.

Inelastic scattering occurs when a projectile interacts with a nucleus and gives it some of its energy, raising it to an excited state. At low energies the nucleus can be exited purely by the Coulomb field between the projectile and the target; this is known as Coulomb excitation and is appreciable only for highly charged projectiles.

The simplest model of inelastic scattering is to assume that the incident particle interacts with one nucleon in the target and promotes it to a higher energy state. The cross-section for this process is proportional to the absolute square of the matrix element.

$$M = \langle \psi_f | V | \psi_i \rangle \tag{2.21}$$

where ψ_i is the wave function of the initial state (incident particle + target), ψ_f that of the final state and V the interaction responsible for the excitation.

Many calculations have been made with this model, and in most cases it has been found that the calculated cross-section is too small.

For rotational nuclei the radius

$$R(\theta,\phi) = R_0 \{1 + \beta Y_2^0(\theta,\phi)\} \tag{2.22}$$

where β is the deformation parameter. The nuclear potential is assumed to depend on the distance from the nuclear surface so that to first order in β

$$V(r - R(\theta,\phi)) = V(r - R_0) - \beta R_0 Y_2^0(\theta,\phi)\frac{dV}{dr} \tag{2.23}$$

The first term is the spherical optical potential between the target and the projectile, and the second gives the coupling potential between the incident and outgoing channels that is the interaction potential.

In the case of vibrational nuclei, the radius is

$$R(\theta,\phi) = R_0\{1 + \sum_m \alpha_m^* Y_2^{m^*}(\theta,\phi)\} \qquad (2.24)$$

where the α_m^* are time-dependent distortion parameters.

If a root-mean-square deformation parameter is $\beta^2 = \langle 0|\sum_m |\alpha_m|^2|0\rangle$, the potential is

$$V(r - R(\theta,\phi)) = V(r - R_0) - \sum_m \alpha_m^* R_0 Y_2^{m^*}(\theta,\phi)\frac{dV}{dr}. \qquad (2.25)$$

The compound nucleus model was introduced by Bohr to explain the narrow resonances observed in experiments with low-energy neutrons. It is assumed that the incident neutron and the target form a compound nucleus in which many of the target nucleons participate collectively and the kinetic energy of the incident neutron is shared with these target nucleons. The participation of many target nucleons is necessary to produce the closely spaced levels of the compound system. On the basis of this many-particle picture, it must take some time for a single nucleon in the compound nucleus to acquire sufficient energy to be emitted and therefore the emission of the excess energy of the compound system in the form of a γ - ray is highly probable.

In the compound nucleus model it is assumed that the mode of decay of the compound nucleus is independent of its mode of formation. A reaction can be represented as a two-stage process

$$A + a \rightarrow C^* \rightarrow b + B$$

where C* is the compound nucleus, and the decay of C^* should not depend on the nature of the projectile *a* and the target *A*. Comparison of the decay of the same compound nucleus formed by different primary interactions have verified this

independence hypothesis in the intermediate energy region. Such comparisons must of course be carried out for the same range of excitation energies.

It is important to distinguish between two types of nuclear interaction, direct and compound. Direct processes occur in the time it takes the incident particle to traverse the target nucleus; this is typically 10^{-21} to 10^{-22} s, depending on the energy and target. Compound processes follow the capture of the incident particle by the target nucleus, and a thorough sharing of its energy among the target nucleons. After a long time a nucleon or group of nucleons near the surface may be a statistical fluctuation, receive enough energy for it to escape, just as a molecule may evaporate from a heated drop of liquid. This process continues until the energy is below the threshold for particle emission and then the nucleus emits gamma–rays until it reaches its ground state. Compound processes take much longer than direct processes, typically around 10^{-16} seconds.

Because of the difference in their time scales, direct and compound processes add incoherently. It is thus possible to calculate their cross-sections separately, and then add them together for comparison with the experimental data. At low energies it is however also possible for the projectile to be captured by the target nucleus to form a compound nucleus that subsequently decays by particle emission.

Compound nucleus reactions are more important at low energies. At low energies the reaction may go through a single state in the compound nucleus to a single state in the final nucleus. The cross-sections of such reactions as a function of energy show a pronounced resonance structure that may be analysed by the Breit-Wigner theory.

For charged particles it is necessary to add the Coulomb amplitude to the Breit-Wigner amplitude and at higher energies there is also direct nuclear amplitude that for elastic scattering can be calculated from the optical model. The formalism may be extended to treat reactions exciting two overlapping levels, but as the mean level spacing D becomes comparable with the mean level width Γ such calculations become impracticable and a statistical approach must be used.

When $\Gamma >> D$, so that the levels overlap strongly, and the energy resolution $\Delta E < \Gamma$, the cross-sections fluctuate as a function of energy, but in so complicated a way that it is not possible to identify the contributing resonances.

If the energy spread $\Delta E >> \Gamma$, many states in the compound nucleus are excited, but the fluctuations are no longer apparent. At low energies these reactions proceed only to discrete states in each residual nucleus R'. As the energy increases it becomes possible to reach the unresolved continuum of states in R', and at still higher energies the cross-section going to the discrete states is negligible and we only need to consider the continuum states. In direct interactions, the projectile retains its full energy and leaves the target nucleus in its ground state. These are called direct or shape elastic scattering. If the projectile gives energy to the target, leaving it in an excited state, the interaction is called **direct inelastic scattering.**

Compound nucleus reactions in which the projectile is captured by the target, which attains statistical equilibrium and then decays by particle and gamma emission. If the emitted particle is the same as the projectile and has its full energy it is called **compound elastic scattering** whereas if it has less than the full energy it is **compound inelastic scattering.**

It is also possible for different particles to be emitted, both by the direct and by the compound processes, and the probability of this happening increases with the incident energy. At low energies each of these reactions leaves the residual nucleus in a particular final state, and the Q value of the reaction determines the threshold energy below which the reaction cannot take place.

2.4 The Compound Nucleus Process

In a nuclear reaction, the incident particle is absorbed by the initial, or target, nucleus to form a compound nucleus. The compound nucleus disintegrates by ejecting a particle or a γ -ray, leaving the final, or product, nucleus.

To illustrate the types of processes that can occur when a nuclear interaction takes place, we shall consider what happens when a proton is incident upon a nucleus. At energies low compared with the Coulomb barrier the proton interacts only with the Coulomb field of the target nucleus, and it is elastically scattered according to

Rutherford's law. At somewhat higher energies it begins to interact with the nuclear field, and then it can be either elastically scattered or absorbed to form the compound nucleus (Bohr 1936). This compound nucleus is in an excited state, and after some time it emits particles until finally reaches the ground state. If few reactions are energetically allowed, a proton may be emitted with the same energy as the incident proton; this is known as **compound elastic scattering**. As the incident energy rises, more and more reaction channels open up, and this process becomes increasingly importable [7].

Even at quite low energies it is also found that some nuclear reactions can take place immediately, without passing through the compound-nucleus stage: these are known as direct reactions. More precisely, a direct reaction may be defined as one that passes at once from the initial to the final state, without any intermediate state.

The character of the reaction depends on the structure of the target nucleus. In the case of reactions on light nuclei, with their well-spaced energy levels, the reaction cross-sections may show marked resonance behavior as the incident energy passes individual states in the compound nucleus. For heavier nuclei the levels are closely spaced and overlapping, so that the resonance structure is averaged out and the cross – sections vary more smoothly with energy [14].

In many of these reactions at medium energies more than two particles are emitted. Nuclear reactions may be classified as compound-nuclear or direct, depending on whether or not they pass through the intermediate compound-nuclear state. Both processes may simultaneously contribute to the reaction in a particular channel. Although the direct particles are emitted immediately and the compound nuclear particles some time later, the time lapse is still very small compared with the resolution of the most refined detecting apparatus. The particles cannot therefore be distinguished experimentally, and so the cross-sections calculated for the two processes have to be combined before comparison is made with the experimental data.

Once a nucleus is excited, it can decay in a variety of ways, by fission, by particle emission, and by beta and gamma decay. The character of the processes of nuclear excitation and decay depends on the type of incident particle and of target nucleus, and this determines the extent to which they are governed by the Coulomb field, or by

the nuclear field or by both together. All reactions are subject to the conservation laws of energy, spin, parity, isospin and baryon number, and studies of the relative intensities of various reaction channels, and of the angular distribution of their cross-sections, yield much detailed information on nuclear structure.

The particles of the highest energy of the same type as the incident particle correspond to elastic scattering and the ones of lower energies to inelastic scattering. For low energies on light nuclei discrete groups of particles at a series of energies are observed, and these correspond to excited states of the target nuclei and enable their energies to be found [12].

At lower emerging energies it is often found, particularly for heavy nuclei with high level densities at rather low excitation energies that the individual states are no longer resolved and merge into a continuum. The corresponding continuum cross-sections can also be analysed by the statistical theory of reactions.

As the bombarding energy increases the character of the reaction changes, and we want to understand this in terms of a simple model. This will enable us to calculate the cross-section and the other features of the reaction, and hence to obtain information on nuclear structure.

At low energies, neutrons and protons interact very differently. Neutrons interact strongly with the nucleus, and can be scattered or captured, whereas protons are repelled by the electrostatic field of the nucleus and are scattered elastically with a cross-section given by Rutherford's formula.

Low energy neutron scattering is strongly affected by the structure of the compound nucleus formed when the neutron is captured by the target. As we have seen, neutron capture gives about 8 MeV to the nucleus, so the compound nucleus is formed with an energy of about $(E_n + 8)$ MeV, where E_n is the energy of the incident neutron in the centre-of-mass system. At this excitation energy, most nuclei have a high density of excited states, and as E_n is increased, these are excited, one by one. As the neutron energy goes through the energy of the excited state of the compound nucleus resonance occurs, so that the scattering and reaction cross-section go through a maximum. The energy at the maximum cross-section corresponds to that of the

excited state, and its width to the lifetime of the state. Between resonances, the elastic scattering cross-section for other processes falls to zero. The angular distribution of the scattering at the resonance tells us the angular momentum J of the excited state of the compound nucleus. Thus by analysing the cross-section of low energy neutron scattering we can determine many of the properties of excited nuclear states.

At somewhat higher energies, approaching that of the Coulomb barrier, the protons can also interact with the nucleus, and we observe rather similar cross-sections showing the combined effects of resonance and Rutherford scattering. As the energy increases still further, the density of states in the compound nucleus increases very rapidly and soon it is no longer possible to resolve the individual resonances. This is not just a matter of the energy resolution of the detecting equipment; the widths of the states also on average increase with excitation energy and eventually with they overlap more and more so that there is no hope of ever resolving them. When this happens the cross-sections become much simpler, and vary quite smoothly with energy.

2.5 Level Width and Nuclear Energy

In the discussion of energy states excited by nuclear reactions it is customary to use, instead of the disintegration constant, a quantity proportional to it called the level width, and defined by the relation, $\Gamma = \frac{h}{2\pi\tau}$

Its use is based on an application of the Heisenberg uncertainty principle. Level widths are usually given in eV; for a wide level, Γ may be of the order of 10^4 eV, as in the case of light nuclei, and the lifetime is 6.6×10^{-20} sec, while a sharp level width of 0.1 eV has the relatively long mean life of 6.6×10^{-15} sec. When the narrow level is that of a compound nucleus, the lifetime of that level can be 10^{-15} s or 10^{-14} s.

Along with the level width, the level spacing D, or mean distance between levels, can be obtained from resonance measurements and is an important quantity in nuclear spectroscopy. The level width and level spacing are useful not only for characterizing compound nuclei, but for any excited nuclear states, and can be applied to both bound and virtual levels.

In medium mass nuclei, the widths are of the order of eV and the spacing of the order of KeV, and in heavy nuclei these magnitudes are substantially reduced. The study of resonance phenomena in nuclear reactions can be seen to have great importance because it provides information about the width and spacing of the energy levels of the compound nucleus. This resonance behaviour persists for incident energies of up to about 1 MeV for heavy nuclei and about 10 MeV for light nuclei.

At low bombarding energies the excited levels of the compound nucleus are discrete and may be widely spaced. This low energy region is therefore called the resonance region. At higher bombarding energies the excited levels in the compound nucleus are more closely spaced, broader, and partially overlapped, so that in this region of overlapping resonances the excitation functions become much smoother functions of energy. This energy region is called **the continuum region**.

In the continuum region the fine structure of the resonances is often not resolved and then excitation functions show broad maxima whose positions vary smoothly and slowly with mass number. These giant resonances have width up to a MeV and spacings of about 10^{-20} MeV.

The dependence of the width and spacing on the mass number and the excitation energy of the nucleus provide the theories of nuclear reactions and nuclear models. The partial widths of a level of the compound nucleus give the relative probabilities for different modes of disintegration, and these probabilities also yield information about nuclear structure.

The concept of level widths is useful because values of these widths can often be obtained from measurement of resonances.

Along with the level width, the level spacing D, or mean distance between levels, can be obtained from resonance measurements and is an important quantity in nuclear spectroscopy. The level width and level spacing are useful not only for characterizing compound nuclei, but for any excited nuclear states, and can be applied to both bound and virtual levels.

2.6 The Statistical Approach

When the compound nuclear states are strongly overlapping any compound nucleus reaction excites a large number of these states and it is necessary to make statistical assumptions to calculate the cross-section [5].

When a nucleon interacts with a nucleus it can be scattered immediately; this is elastic scattering, if it loses no energy and inelastic scattering if it gives energy to the nucleus.

We can express the cross-section of a compound nucleus reaction $\sigma_{\alpha\beta}$ from the α to the β channel as a product of the cross-sections for the formation of the compound nucleus from the channel α and the probability of the decay into the channel β,

$$\sigma_{\alpha\beta} = \sigma_{\alpha}(CN)P_{\beta} \qquad (2.26)$$

In the region where the widths of the resonances are of the order of their spacing an incident neutron can excite several compound states whose relative phases will depend on the mode of excitation.

If the energy of the incident particle is sufficient to excite the system high in the continuum region where the density of overlapping levels is very high and a very large number of states are excited simultaneously, the phase relations between these states may be regarded as random at least with regard to the effect on the modes of decay.

If the compound nucleus is sufficiently long-lived, thermodynamic equilibrium is set up and the distribution of the available energy follows the laws of statistical mechanics.

The assumption that this equilibrium situation is reached is the basis of the statistical model; it is assumed that the energy and total angular momentum determine the properties of the compound nucleus so that, apart from the energy dependence, all possible decay modes occur with equal probability.

In the continuum region many channels are open for the decay of the compound state and the probability of re-emission through the entrance channel is very small and

therefore compound elastic scattering is negligible. In this non-elastic region the wave function of the incoming neutron will be attenuated so that

$$U_o(r) = e^{-iKr}, \qquad r \le R \tag{2.27}$$

where K is the wave number in the internal region.

The absorption cross-section is given by

$$\sigma_{abs} = \frac{\pi}{k^2}\sum_l (2l+1)(1-|S_l|^2) \tag{2.28}$$

$$\sigma_{CN}(\alpha) = \frac{\pi}{k^2}(2l+1)(1-|S_\alpha|^2) = \frac{\pi}{k^2}(2l+1)T_\alpha \tag{2.29}$$

where $T_\varepsilon = 1-|S_\varepsilon|^2 = \dfrac{4kK}{(k+K)^2}$ is called the transmission coefficient for S-wave neutrons.

Therefore the cross-section for the formation of the compound nucleus can be represented by

$$\sigma_{CN}(\alpha) = \sigma_{abs} = \frac{\pi}{k^2}\frac{4kK}{(k+K)^2} \tag{2.30}$$

and the cross-section for a particular channel reaction is

$$\sigma_{\beta\alpha} = \frac{\pi}{k^2}\frac{4kK}{(k+K)^2}\frac{\Gamma_\beta}{\Gamma} \tag{2.31}$$

At low energies, $\sigma_{abs} = \dfrac{4\pi}{kK} \propto \dfrac{1}{v}$ (2.32)

Yielding the 1/ v law for low energy neutron capture.

If $\overline{\Gamma}_{\cdot}$ is the mean width for resonances due to particles in channel α and D is the mean spacing of level within an energy interval I it can be written by

$$\sigma_{CN}(\alpha)=\frac{1}{I}\int_{E-\frac{1}{2}I}^{E+\frac{1}{2}I}\frac{\pi}{k^2}\sum_s\frac{\Gamma^s\Gamma_\alpha^s}{(E-E_n)^2+(\frac{1}{2}\Gamma)^2}dE \tag{2.33}$$

$$\sigma_{CN}(\alpha)=\frac{\pi}{k^2}\frac{2\pi}{I}\sum_s\Gamma_\alpha^s=\frac{\pi}{k^2}2\pi\frac{\overline{\Gamma_\alpha}}{D} \tag{2.34}$$

$$\frac{\overline{\Gamma_\alpha}}{D}=\frac{1}{2\pi}\frac{4kK}{(k+K)^2}\approx\frac{2k}{\pi K} \tag{2.35}$$

In order to compare data at different excitation energies it is convenient to define in energy independent quantity called the s-wave strength function as

$$\frac{\Gamma_\alpha^o}{D}=(\frac{E_0}{E})^{1/2}\frac{\overline{\Gamma_\alpha}}{D} \tag{2.36}$$

where E_0 is an arbitrary energy taken to be 1 eV. $\sigma_{\alpha\beta}$ and σ_{abs} can be related to the reflection coefficients and s-matrix elements, but these coefficients must reproduce the rapid fluctuations in the cross-sections due to the resonances and are therefore very complicated functions energy comparison of equation

$$\sigma_{CN}(\alpha)=\frac{\pi}{k^2}\frac{4kK}{(k+K)^2} \tag{2.37}$$

and equation

$$\sigma_{abs}=\frac{\pi}{k^2}\sum_l(2l+1)(1-|S_l|^2) \tag{2.38}$$

then yields the expression for the transmission coefficient

The over-all transmission coefficient can be represented by

$$T_\alpha \approx \frac{4k}{K} P_a \tag{2.40}$$

where P_a is a Gamow-type penetration factor for the Coulomb barrier and centrifugal barrier, and $\frac{4k}{K}$ is the probability that the incident particle can pass successfully from outside the nucleus, where its wave number is k, to the region inside the nucleus, where its wave number is K (>> k).

According to the Reciprocity Theorem, the cross-section of the time –reverse of a reaction is

$$\sigma_{\alpha\beta} = \sigma_{\beta\alpha} = \sigma_\beta(CN)\, P_\alpha \tag{2.41}$$

$$T_\alpha P_\beta = T_\beta P_\alpha \tag{2.42}$$

This is true for all channels α and β and

$$\frac{P_\alpha}{T_\alpha} = \frac{P_\beta}{T_\beta} = \xi \tag{2.43}$$

where ξ is a constant. The probability to a reaction in a particular channel is proportional to the transmission coefficient in the channel.

$$\sum_\alpha P_\alpha = 1 = \sum_\beta P_\beta \tag{2.44}$$

$$\sum_\alpha P_\alpha = \xi \sum_\alpha T_\alpha \tag{2.45}$$

and therefore

$$P_\beta = \xi\, T_\beta = \frac{T_\beta}{\sum_\alpha T_\alpha} \tag{2.46}$$

and so

This formula for the compound nucleus cross-section tells us that the cross-section is proportional to the production of the transmission coefficients in the entrance and exit channels. In the case of neutron and proton elastic scattering at low energies both the direct and the compound nucleus processes contribute.

The compound nucleus cross-section of a reaction to a particular final state usually rises rather rapidly immediately above threshold, reaches a maximum at a few MeV above threshold, and then falls due to the competition from other channels as their thresholds are also passed. The direct cross-section however, rises gradually from threshold and attains a much broader maximum at energies many MeV above threshold. This difference in behaviour can be used to separate the compound and direct contributions to the cross-section.

When the energy of the incident neutron is about 1 MeV or higher, new types of processes can occur, such as inelastic scattering and the emission of charged particles. The emitted neutrons can have the residual nucleus in excited states so that some of the scattering is inelastic rather than elastic [12].

CHAPTER 3

NUCLEAR CROSS-SECTIONS

3.1 Nuclear Reaction Cross Sections

The relative yield of ejected particles for a given incident flux is influenced by certain external factors such as the physical form of the target material and the target thickness [10]. It is therefore desirable to define concepts which are independent of these external factors and are a measure of the tendency of a nucleus to undergo nuclear reactions. For this purpose it is useful to define the total cross section of nuclides as the effective area presented by the nucleus to the beam. Essentially we assign to each nucleus an equivalent fictitious disk, whose face is perpendicular to the beam and whose area is such that the total number of particles which would fall on the fictitious disk if the incident particles maintained their original trajectories is equal to the total number actually removed from the beam as a result of nuclear collisions [6].

The number of scattered particles presented to a beam by a thin target is

$$N_S = \frac{N_A \rho S \Delta x}{M} \tag{3.1}$$

where N_A is Avogadro's number, S the area of the beam, Δx the thickness, ρ the density, and M the gram-atomic weight of the target material. Defining the beam intensity I as the number of particles crossing a unit area per unit time, we make the fundamental assumption that the change of intensity due to the thin layer is related to the original intensity simply as the effective area presented by all the scattered particles is to the total area of the beam. According we take as the definition of the total cross section σ of a single nucleus

$$\frac{\Delta I}{I} = \frac{-\sigma N_S}{S} = \frac{-\sigma N_A \rho}{M} \Delta x = -\sigma \eta \Delta x = -\mu \Delta x \tag{3.2}$$

where η is the number of target nuclei per unit volume. The product $\mu = \sigma\eta$ is called the linear absorption coefficient. The product $\rho\Delta x$ measures in milligrams per square

centimeter is sometimes called the "thickness" of the target. A convenient unit for nuclear cross sections is 10^{-24} cm^2, which is called a barn.

In principle, to obtain an experimental cross section for particles of a given energy, it is necessary to measure only the fractional change in the intensity of a monoenergetic beam caused by a thin layer of known thickness. We use a thin layer to minimize the error due

$$\sigma = \frac{n}{IN_S} \tag{3.3}$$

If several independent processes occur which can be experimentally distinguished by the nature or energy of the scattered or ejected particles, we may decompose the total cross section into partial cross sections for the various processes. Accordingly we set

$$\sigma = \sigma_1 + \sigma_2 + \sigma_3 + \ldots = \sum_i \sigma_i \tag{3.4}$$

where the partial cross section for i^{th} process is

$$\sigma_i = \frac{n_i}{IN_s} \tag{3.5}$$

and n_i is the number of processes or particles of the i^{th} type per unit time.

Experiments indicate that the transmission of neutrons or gamma rays through moderately thick layers of target material obeys quite well a relation which may be deduced immediately if we assume that only single collision processes take place. It follows from this assumption that the energy of the particles in the beam at any depth x in the material is constant. Treating σ, therefore, as a constant, letting ΔI be a differential, and letting I_0 be equal to the intensity at $x = 0$, we may integrate Eq (3.2) to obtain

$$I = I_0 \exp(-\sigma\eta x) = I_0 \exp(-\mu x) \tag{3.6}$$

The measurement of the ratio between the intensity transmitted through a known thickness of target material and the original intensity, in conjunction with a

determination of η, thus leads to a value for the total cross section. Most measurements of cross sections for neutrons and gamma rays make use of thick targets and are based upon Eq (3.6).

In order to derive accurate cross sections from the intensity data obtained in such measurements, considerable care must be taken to establish the energy homogeneity of the source, the purity of the absorber, and the efficiency of the detector. Furthermore careful design of the geometry of the apparatus is necessary to minimize the unwanted scattered particles which enter the detector or to make it possible to current for these particles.

Experimental data are now available giving the relationship of neutron cross section vs. energy for various substances for the kinetic energy range from 0.001 eV to around 20 MeV. The low-energy-neutron data (0.001 to 100 eV) have been obtained by using time-of-flight methods and crystal spectrometers. The data for medium-fast neutrons (10 keV to 3 MeV) have been obtained using neutrons from the $^{7}Li(p, n)^{7}Be$, the $^{12}C(d, n)^{13}N$, and the $D(d, n)^{3}He$ reactions where the incident deuterons or protons are accelerated by an electrostatic generator. By carefully regulating the incident beam, by limiting the angle subtended by the target, it has proved practical to limit energy spread of the neutron beam in this region to as low as 1 keV. To avoid sacrificing intensity, however, a greater energy spread is usually used.

The experimental neutron-cross-section data indicate that there are large fluctuations in the relationships of neutron cross section vs. energy, particularly in the low-energy region and for lighter nuclides. We get the neutron cross sections which show these large fluctuations or resonances. Certain general statements can be made concerning the spacing of these rapid fluctuations in the neutron cross section of the typical nuclides. The resonances in light nuclides ($A<50$) and in certain special heavy nuclides such as Bi, Pb, and Sn are few and widely spaced in the region below 1 MeV. The spacing, however, decreases very rapidly with increasing A, and for $A>65$ the spacing is so small that the current data indicate only a continuous variation of cross section with energy. We have already indicated that these resonances associated with the excited states of the compound nucleus which are formed by neutron capture.

Apart form the resonances there appear to exist certain regularities in total neutron cross sections. The nuclear cross sections are sometimes given in terms of nuclear areas, which are computed from $R = 1.45^{1/3} \times 10^{-13}$ cm. The $\sigma(T, A)$ surface reveals that neighboring nuclides show similar variations with energy, but the shape of the sectional curves changes gradually with A so that nuclides differing greatly in A have cross- section curves which differ quite markedly. An interesting feature of this surface is the fact that the peak cross section, which occurs at low energies for the heavy elements.

As a result of interactions with atomic electrons, charged particles in passing through the matter lose energy; hence precise cross- section measurements for protons, deuterons, alpha particles, etc., must be made with relatively thin targets and must be based upon the detection of ejected or scattered particles rather than the minute intensity change upon transmission through the target. Accordingly, the experiment leads directly to the partial cross section rather than the total cross section

When the residual nucleus of a reaction induced by charged particles is radioactive, the convenient method of stacked foils is available for measuring the cross section as a function of the incident particles. In this method the absorber is an assembly of thin layers of a particular type of target material. After exposure to the beam these layers are disassembled, and the disintegration rates of various layers are determined by means of counters which are sensitive to the disintegration products of the radioactive residuals. The intensity available at each layer may be assumed to be approximately constant as long as the total target thickness is small compared to the mean range of the particles in the target material. It can be shown on the basis of the laws of radioactivity that the relative activities or disintegration rates at a given time after the bombardment are proportional to the original numbers of radioactive products formed in each layer during the bombardment. Since the intensity is the same for each layer, the activities, when plotted against the corresponding energies, give directly the relative cross sections as a function of energy. With careful calibration of the various components in these experiments, it is possible to obtain absolute cross sections by the method as well. If several chemically separable types of radioactive residuals are produced, partial cross sections for the different processes can also be established.

Most experiments designed to establish partial cross sections are based upon the measurement of the intensity distribution of ejected or scattered particles from thin targets as a function of the angles θ_l and ρ_l. This distribution may be characterized by a function $\sigma(\theta_l, \rho_l)$, known as the differential cross section per unit solid angle which is defined by

$$\sigma_l(\theta_l,\rho_l)\,\Delta\Omega_l = \Delta n/Ins \tag{3.7}$$

where

$$\Delta\Omega_l = \sin\theta_l\,\Delta\theta_l\,\Delta\rho_l \tag{3.8}$$

is an element of solid angle and Δn is here the number of ejected or scattered particles per unit time which go into $\Delta\Omega_l$. The solid-angle interval $\Delta\Omega_l$, which is determined by the sensitive area of detector and the distance of the detector from the target according to

$$\Delta\Omega_l = \text{area of window}/R^2 \tag{3.9}$$

must be small enough so that the change in $\sigma_l(\theta_l,\rho_l)$ is small over the range of angles subtended by the detector window. Not only is the differential cross section per unit solid angle a useful intermediate concept in the experimental determination of partial cross sections, but in addition it has a direct physical significance in nuclear physics which is becoming more and more important as nuclear physics develops. This importance stems form the sensitivity of $\sigma_l(\theta_l, \rho_l)$ to the nature of nuclear forces. Thus the agreement between experimental and theoretical differential cross sections per unit solid angle for all energies and all nuclei would provide a very convincing "proof" of the theory which yields the theoretical function.

The theoretical analysis of collision phenomena is greatly simplified if we use the center-of-mass coordinate system. In this system the total energy of the system, apart from the constant initial rest energy, is the total kinetic energy of the incident particle and the scatterer. The total kinetic energy may be expressed as

$$T = 1/2\, m_r v^2 = p^2/2m_r \tag{3.10}$$

where

$$m_r = M_m/M + m \tag{3.11}$$

and by definition

$$p = m_r v \tag{3.12}$$

In effect we have transformed our two-body problem into an equivalent one-body problem in which the center of mass serves as an infinitely heavy scattered particles and the incident particle has the mass m_r and velocity v. If the ejected particle is different from the incident particle or has a different energy (i.e., if a nuclear reaction or inelastic scattering occurs), the final system is equivalent to an infinitely heavy scatterer and a particle with the mass

$$m'_r = m' M' /M' + m' \tag{3.13}$$

and with the kinetic energy

$$T' = \tfrac{1}{2} m'_r v'^2 = p'^2/2m'_r \tag{3.14}$$

where T' is the kinetic energy of ejected particle.

In view of the independence of the different scatterers the ratio $\Delta n / N_s$ in Eq. (3-7) is simply the number of particles per unit time scattered by a single scatterer into the solid angle $\Delta\Omega_l$. Thus in the theoretical derivation of the differential cross section we may pretend that there is only one scatterer in the beam. In order to define a theoretical concept which corresponds to the experimental quantity defined by Eq (3.7), we must use the basic connection between statistics and probability. According to this connection, when dealing with ratios of large numbers of particles, we may replace numbers of particles by probabilities for a single particle, or numbers per unit time by probabilities per unit time. Consequently we may accept for the basic definition of the theoretical cross section in the center-of-mass system

$$\sigma(\theta,\rho)\,\Delta\Omega = w/\vartheta \tag{3.15}$$

where w represents the probability per unit time for scattering or transition into $\Delta\Omega$ due to a single scattered particle and ϑ represents the incident probability per unit area per unit time.

Two integrated concepts follow directly from the theoretical cross section per unit solid angle. These are

$$\sigma(\theta) = \int_0^{2\pi} \sigma(\theta,\varphi)d\varphi \qquad (3.16)$$

which relates to the probability per unit time of scattering between the cones defined by θ and $\theta + \Delta\theta$, and the total cross section

$$\sigma = \int_0^{2\pi} \int_0^{\pi} \sigma(\vartheta,\psi)(\sin\vartheta)d\theta d\psi \qquad (3.17)$$

which relates to the probability of scattering in any direction.

3.2 The Elastic Cross-Sections and Total Cross-Sections

It was shown that at moderate energies when the effects of the individual states of the compound nucleus on the scattering are no longer resolved the cross-sections for the elastic scattering of nucleons by nuclei vary rather smoothly with energy and from one nucleus to the next [7].

Using this model, the expressions for the absorption and elastic cross-section for neutrons incident on a nucleus of radius R can be expressed by

$$\sigma_A = \pi R^2\left[1 - \left\{(1+2KR)e^{-2kR}\right\}/2K^2R^2\right] \qquad (3.18)$$

$$\sigma_E = 2\pi\int_0^R \left|1 - \exp(-K + 2ik_1)s\right|^2 \rho d\rho \qquad (3.19)$$

where $s^2 = R^2 - \rho^2$. The absorption coefficient K is related to the nuclear parameters by

$$K = \frac{3A\sigma}{4\pi R^2} \qquad (3.20)$$

where σ is the mean cross-section for nuclear collisions.

$$\sigma = \{ Z\sigma_{np}\alpha_{np} + N\sigma_{nn}\alpha_{nn} \} / A \tag{3.21}$$

The coefficients σ_{np} and σ_{nn} allow for the reduction in the cross-section due to the Pauli principle that occurs because some final states are already occupied.

The total absorption cross-section from the total measured flux, is

$$\sigma_A = -\int_0^{2\pi}\int_0^{\pi} \frac{i\hbar}{2mV}\left(\dot{\psi}\frac{\partial\psi}{\partial r} - \psi\frac{\partial\dot{\psi}}{\psi r}\right) r^2 \sin\theta \, d\theta \, d\phi. \tag{3.22}$$

Now the wavefunction

$$\psi = -\sum_L \frac{(2L+1)}{2ikr}\rho_L(\cos\theta)(S_L e^{ikr} - e^{-ikr}) \tag{3.23}$$

where

$$S_L = e^{2i\delta_L} \tag{3.24}$$

and hence

$$\sigma_A = \frac{\pi}{k^2}\sum_L (2L+1)(1 - |S_L|^2) \tag{3.25}$$

The total cross-section is the sum of the total elastic cross-section σ_E and total absorption cross-section σ_A, so that

$$\sigma_T = \frac{2\pi}{k^2}\sum_L (2L+1)(1 - \mathrm{Re}\, S_L) \tag{3.26}$$

3.3 Resonance Theory for Nuclear Cross- Sections

For low-energy projectiles these fluctuations consist of high, narrow peaks which are called resonances. At very low energies charged particles do not cause nuclear reactions because of the large coulomb barrier, but resonance behaviour is observed in

low energy neutron scattering from medium mass nuclei and in neutron capture, or (n,γ) reactions on heavy nuclei. These resonances are exceedingly sharp [12].

The formation of a resonance at particular incident energy may be associated with the formation of a long-lived state of the compound system composed of the projectile and the target.

Since the projectile carries kinetic energy the total energy of the compound system is positive and the state of the system is a virtual or quasi-stationary state and not a true stationary state. This mean that the state of the compound system must eventually decay with emission of the original particle, a different particle, or a γ- ray.

The incident projectile was assumed to move in an attractive real potential so that the quasi-stationary levels are the single particle levels in this potential with energy, and a resonance will occur whenever the incident energy corresponds to the energy of one of these single-particle levels. For a simple square well potential of depth V_0 and range R, the s-wave resonances occur when $KR = (n + \frac{1}{2})\pi$ where $K^2 = 2\mu(E + V_0)/\hbar^2$, and p-wave resonances occur when $KR \approx n\pi$.

For a given nucleus the spacing of these levels is about 10 MeV, depending on the choice of potential parameters. If it is assumed that, for low energies, V_0 is independent of mass number A while $R \propto A^{1/2}$, the positions of the resonances can be located as functions of A for fixed incident energy. It is evident that this model contains many of the features associated with giant resonances but apparently contains none of the features associated with the fine resonances. If the fine resonances are also to be associated with quasi-stationary levels, the levels must be closely spaced levels of a many particle system and assume that many nucleons participate in the formation of the compound system.

Resonance is important in nuclear reactions because knowledge of the resonance energies in a reaction yields information about certain energy levels of the nucleus. The concepts of cross-section and level width can be applied to resonances in a quantitative way.

In the important case of resonance processes, a theoretical formula for the cross-section was derived by Breit and Wigner. The Breit and Wigner formulas give a good description of the energy dependence for both the reaction cross-section and the scattering cross-section in the vicinity of a single isolated resonance level.

The compound nucleus may be said to exist in a "quasi-stationary" state, which means that although it exists for a time interval which is very long compared with the natural nuclear time, it can still disintegrate by ejecting one or more nucleons. These quasi-stationary states are called virtual states or virtual levels in contrast to bound states or bound levels, which can decay only by emitting γ radiation. There are many possible virtual levels of the compound nucleus. These levels are closely related to the phenomenon of resonance.

The occurrence of a resonance peak in the rate of a nuclear reaction when the energy of the incoming particles is varied shows that the compound nucleus has an energy level whose excitation energy is very nearly the sum of the binding energy of that particle and its kinetic energy.

Each excited states of the compound nucleus, whether bound or virtual, has a certain mean lifetime τ; there is a certain period of time, on the average, during which the nucleus remains in a given excited state before decaying by emission of either a particle or a γ ray.

The study of resonance phenomena in nuclear reactions can now be seen to have great importance because it provides information about the width and spacing of the energy levels of the compound nucleus.

In many cases, the strong resonance maxima of neutron capture were found to be unaccompanied by maxima in the scattering cross-section. The important experimental fact dictated a major revision in the resonance model which had appeared to be satisfactory for the (α, p) resonance reactions. It was necessary to account for strong resonance capture of the slow neutron and at the same time, to be able to account for a very small probability for reemission of the neutron.

Breit and Wigner showed that this could be accomplished if the compound level has a higher probability of decay by other modes that by reemission of the neutron. The compound nucleus thus corresponds to a damped oscillator, accepting the incident neutron readily at its resonance energy, but dissipating this energy mainly by γ ray transitions to lower levels of the compound nucleus, as in the (n, γ) reactions. This model is often referred to as the dispersion theory of nuclear reactions because of its parallelism with the theory of the dispersion of optical light. The compound nucleus becomes, in this model, an intermediate state in which the excitation energy can be shared by several nucleons and from which de-excitation can occur in a variety of competing modes.

In low and intermediate energy, intermediate nuclei, the most important reactions between neutrons of low or intermediate energy and nuclei of intermediate atomic weight are elastic scattering (n, n) and radiative capture (n, γ). The total cross section (σ_t) and the radiative capture cross section σ (n, γ) have been measured as functions of the incident neutron energy. At neutron energies where there is no resonance, this cross section represents the probability that the neutrons are scattered without the formation of a compound nucleus. In this case, the nucleus acts like a hard sphere of radius R, and it has been shown that for neutrons with energies up to about 1 MeV the scattering cross section is

$$\sigma_s = 4\pi R^2 \tag{3.27}$$

This type of scattering is called **potential scattering**.

One part of the low energy, thermal energy region, has a special property in the case of the (n, γ) reaction. Although the Breit – Wigner formula is strictly valid only near a resonance, it may be applied in the thermal energy region in the absence of a resonance if it is assumed that the energy E_o is the resonance energy nearest to the thermal region. All of the factors in the Breit – Wigner formula are constant compared with Γ_n, which is proportional to the neutron velocity v, and λ, which is proportional to 1/v. The (n ,γ) reaction reduces to

$$\sigma(n,\gamma) = \frac{\text{constant}}{v} \tag{3.28}$$

and the cross section for radiative capture is inversely proportional to the neutron velocity.

The only reactions possible for low–energy neutrons on heavy nuclei are, with a few exceptions, elastic scattering and radiative capture. When the positive charge of the nucleus is large, the effect of the Coulomb barrier prohibiting the emission of charged particles of low energy is even greater than with intermediate nuclei. In reactions between low-energy neutrons and heavy nuclei, the cross-sections often show resonances very close together in energy.

The level distances are often of the order of 10 to 100 eV and the excited states of the compound nuclei in this region are usually close together. In heavy nuclei, the resonances are mainly capture rather than scattering resonances, and the neutron width Γ_n is small compared with the radiation width Γ_γ. The total cross-section is practically equal to the capture cross-section $\sigma(n,\gamma)$ near resonance; between resonances, the total cross section is approximately equal to the potential scattering cross section, $4\pi R^2$. At thermal energies, in the absence of resonances $\sigma(n,\gamma)$ follows the 1/v law, as was the case with intermediate nuclei.

In the intermediate energy region, the reactions are similar in nature to those with intermediate nuclei. Resonance scattering is more important than resonance capture and $\Gamma_n > \Gamma_\gamma$. The spacing between resonances, however, is smaller than for intermediate nuclei. It is hard to explore the intermediate energy region because of experimental difficulties with neutrons of these energies. Individual resonances cannot be resolved and the experiments give information about cross sections averaged over many resonances.

The Breit–Wigner formula is averaged over many resonance levels and applied to (n,γ) reactions at neutron energies of about 1 MeV , it is found that the averaged (n,γ) cross section is given by

$$\overline{\sigma(n,\gamma)} = (\lambda^2/2)\ (\Gamma_\gamma/D) \qquad (3.29)$$

where D is the level spacing.

When the energy of the incident neutron is about 1 MeV or higher, new types of processes can occur, such as inelastic scattering and the emission of charged particles. The emission of neutrons is more probable than that of charged particles because of the Coulomb barrier. The emitted neutrons can leave the residual nucleus in excited states so that some of the scattering is inelastic rather than elastic. The cross sections for the reactions in which charged particles are emitted are much smaller than those for inelastic scattering and radiative capture, especially when the target nucleus has a high value of Z, because of the effect of the Coulomb barrier.

The scattering of neutrons with energies greater than 10 MeV has been used to determine values of the nuclear radius. According to theory, the total cross section at high energies approaches the value

$$\sigma_t = 2\pi R^2 \tag{3.30}$$

3.4 Continuum Theory of Nuclear Cross-Sections

At higher bombarding energies (1 to 30 MeV) the individual levels of the compound nucleus become broader and also more closely spaced. The continuum theory of nuclear cross section, which is applicable in this energy domain, is an average over many resonances [12].

These theories can be represented by the expression

$$\sigma_{com} = \pi\lambda^2 \sum_{l=0}^{\infty} (2l+1)\, P_l\ \xi_l \tag{3.31}$$

where P_l denotes the probability that an incident particle whose angular momentum is l will reach the nuclear surface and ξ denotes the probability that the particle will enter and remain in the nucleus.

In the continuum theories internal elastic scattering is explicitly excluded. Elastic scattering is proportional to $(1-\xi)$ and is visualized in terms of an incident particle which never merges with the target nucleus.

The continuum theories of nuclear reaction cross sections were undergoing major revisions, in order to match systematic trends which had been found in neutron cross

sections. That theory deals explicitly with neutron-induced reactions only. The energy dependence of nuclear cross sections, averaged over individual fluctuations and resonances, is expressed in terms of two parameters of the inner nuclear structure. These are nuclear radius R and the wave number K of the incident neutron after it is in the interior of the compound nucleus.

The wave number K for neutron within the nucleus becomes $K^2 = K_0^2 + k^2$ where k is the wave number of the incident neutron as it approaches the nucleus and K_0 is the interior wave number K if the bombarding energy is zero.

At large energies, where $\lambda\!\!\!^{-} \equiv 1/k << R$, the theoretical absorption and scattering cross sections for neutrons are both found to approach the same asymptotic value

$$\sigma_{abs} = \sigma_{sc} = \pi(R + \lambda\!\!\!^{-})^2 \tag{3.32}$$

Therefore the total cross section, for high – energy neutrons, becomes

$$\sigma_t = \sigma_{abs} + \sigma_{sc} = 2\pi(Rt + \lambda\!\!\!^{-})^2 \tag{3.33}$$

The elastic scattering referred to here is purely potential scattering, as internal or resonance elastic scattering is usually explicitly excluded in continuum theories of nuclear cross sections.

3.5 Resonance Reactions and Fluctuating Cross-Sections

The cross section for formation of the compound nucleus can be represented as the maximum cross section times the probability for transmission through the nuclear barrier and the nuclear surface by a particle a , with orbital angular momentum *l*.

For elastic scattering, the maximum possible cross section occurs when the scattering potential reverses the phase of the outgoing (e^{ikr}) portion of the total (partial) wave. The maximum possible elastic scattering cross section is

$$(\sigma_{sc})^l_{max} = 4\pi(2l+1)\lambda\!\!\!^{-2} \tag{3.34}$$

when there is some absorption, the absolute value of the amplitude of the outgoing (e^{ikr}) portion of the total wave is reduced.

In the limiting case of maximum absorption, the amplitude of the outgoing (e^{ikr}) portion of the total wave is reduced to zero. This is one-half of the change in amplitude involved for maximum scattering. The maximum absorption cross section which depends on the difference between the square of the ingoing (e^{-ikr}) amplitude and the outgoing (e^{ikr}) amplitude, is one fourth of the scattering equation, or

$$(\sigma_{abs})^{l}_{max} = \pi(2l+1)\lambda^2 \qquad (3.35)$$

For the important special case of slow neutrons, which can involve only s-wave collisions ($\ell = 0$), the maximum possible reaction cross section becomes simply $\pi\lambda^2$, and therefore it can be enormously larger than the geometrical cross section of the target nucleus.

The elastic scattering cross-section is given by the absolute square of the scattering amplitude

$$f(\theta) = \frac{1}{2ik}\sum_{L}(2L+1)(e^{2i\delta_L} - 1)\,P_L(\cos\theta) \qquad (3.36)$$

and so if a resonance occurs in a particular partial wave it is given by the variation of the appropriate phase shift δ_l with energy. At the resonance energy E_R the cross-section has a maximum value. The energy variation of the phase shift is

$$\delta = \frac{\pi}{2} - (E_R - E)\frac{d\delta}{dE} \qquad (3.37)$$

The value of $\frac{d\delta}{dE}$ determines the sharpness of the resonance.

A width Γ is

$$\Gamma = 2\left(\frac{d\delta}{dE}\right)^{-1} \qquad (3.38)$$

the total elastic cross-section becomes

$$\sigma_E^L = \frac{\pi}{k^2}(2L+1)\frac{\Gamma^2}{(E_R - E)^2 + \frac{1}{4}\Gamma^2} \qquad (3.39)$$

This is the Breit-Wigner formula for the cross-section of a single isolated resonance in the elastic channel when all other channels are closed.

At low energies and for light nuclei the resonances are well separated and the scattering can be analysed to give the energies and widths of the corresponding states in the compound nucleus. For low energy neutrons only s-waves contribute to the scattering and so the radial wave equation outside the nucleus becomes

$$\frac{d^2U}{dr^2} + k^2U = 0\ , \qquad (r > R) \qquad (3.40)$$

So that

$$U(r) = A\sin(kr + \delta_0) \qquad (3.41)$$

The nucleus gives $\frac{RU'}{U} = f(R)$ at r = R and continuity then requires

$$f(R) = kR\ \cot(kR + \delta_0) \qquad (3.42)$$

and the elastic scattering cross-section for s- wave is

$$\sigma_s = \frac{\pi}{k^2}\left|1 - e^{2i\delta_0}\right|^2 \qquad (3.43)$$

At low energies the wave function is very small inside the nucleus so $f \to \infty$ and

$$\sigma_s \approx \frac{\pi}{k^2}\left|1 - e^{-2ikR}\right|^2, \quad (E \to 0) \qquad (3.44)$$

Since $kR << 1$ this becomes

$$\sigma_s = \frac{\pi}{k^2}\left|2ikR\right|^2 = 4\pi R^2, \qquad (E \to 0) \qquad (3.45)$$

As the phase shift δ_0 varies with energy, the function f(R) passes through zero when $kR + \delta_0 = \frac{\pi}{2}$.

At a bombarding energy E, which is in the neighborhood of a resonance E_R, the shape of the resonance by a function f(E) is given by

$$f(E) = \frac{C}{(E - E_R)^2 + (\frac{\Gamma}{2})^2} \tag{3.46}$$

We can expand f(E) about the resonance energy as

$$f(E) = (E - E_R)(\frac{df}{dE})_{E=E_n} + \ldots\ldots\ldots \tag{3.47}$$

Then the scattering cross-section is

$$\sigma_s = \frac{\pi}{k^2}\left|1 - e^{2ikR} - \frac{i\Gamma}{(E - E_n) + \frac{1}{2}i\Gamma}\right|^2 \tag{3.48}$$

The partial width for re-emission of the incident neutron through channel α as

$$\Gamma_\alpha = \frac{2kR}{a}, \tag{3.49}$$

the total width as

$$\Gamma = 2(b + kR)/a \ , \tag{3.50}$$

and the reaction width as

$$\Gamma_r = \sum_{\beta \neq a} \Gamma_\beta = \Gamma - \Gamma_a = \frac{2b}{a} \ . \tag{3.51}$$

Thus the scattering cross-section becomes

$$\sigma_s = \frac{\pi}{k^2}\left|1 - e^{2ikR} - \frac{2ikR/a}{(E-E_n)+i(b+kR)/a}\right|^2 \qquad (3.52)$$

. Thus the scattering amplitude consists of a non-resonant part.

$$A_{pot} = \frac{1}{2ik}(e^{2ikR} - 1) \qquad (3.53)$$

which is the amplitude for potential or **shape-elastic scattering**. The resonant part is

$$A_{res} = \frac{1}{2ik}\left[\frac{2ikR/a}{(E-En)+i(b+kR)/\ a}\right] \qquad (3.54)$$

which represents the scattering arising from re-emission of the absorbed neutron by the compound nucleus or compound-elastic scattering. The cross-section for compound elastic scattering becomes

$$\sigma_{ce,\alpha} = \frac{\pi}{k^2}\frac{\Gamma_\alpha^2}{(E-E_n)^2 + (\frac{1}{2}\Gamma)^2} \qquad (3.55)$$

which is the Breit - Wigner formula for l=0 and the absorption cross-section becomes

$$\sigma_{abs} = \frac{\pi}{k^2}\frac{\Gamma_f\Gamma_\alpha}{(E-E_n)^2 + (\frac{1}{2}\Gamma)^2} \qquad (3.56)$$

The cross-section for compound nucleus formation is

$$\sigma_{cn}(\alpha) = \sigma_{abs} + \sigma_{ce,\alpha} = \frac{\pi}{k^2}\frac{\Gamma\Gamma_\alpha}{(E-E_n)^2 + (\frac{1}{2}\Gamma)^2} \qquad (3.57)$$

and the cross-section for the process $\alpha \rightarrow \beta$ is

$$\sigma_{\beta\alpha} = \frac{\pi}{k^2}\frac{\Gamma_\beta\Gamma_\alpha}{(E-E_n)^2 + (\frac{1}{2}\Gamma)^2} \qquad (3.58)$$

These formulas are the one-level dispersion formulae introduced by Breit and Wigner. At low energies and far from resonance the scattering cross-section is $4\pi R^2$. Near resonance the potential scattering interferes to give the cross-section for compound nucleus formation reduces to $4\pi\Gamma_\alpha/k^2\Gamma$.

If there is only one decay channel apart from the elastic channel, and its width is large, the resonant cross-section takes a particularly simple form. Thus for neutron capture or (n,γ) reactions $\Gamma_\gamma >> \Gamma_n$, so that at resonance

$$\sigma_s \sim \frac{4\pi}{k^2}\frac{\Gamma_n}{\Gamma_\gamma} \qquad (3.59)$$

At higher energies the level density in the compound nucleus increases very rapidly, until the average level width exceeds the level spacing, and then the individual levels are no longer resolved. At still higher energies the fluctuations in the cross-section crowd more and more closely together until finally they are no longer resolved experimentally and the cross-section appears to vary smoothly with energy. The S matrix element is expressed as a sum of an averaged value that varies smoothly with energy and a fluctuating component.

$$s = < S > + S$$

where the notation, < >, indicates energy averaging over an interval sufficiently large to smooth out the fluctuations and yet still small compared with the energy itself. The energy-averaged matrix element < S > is the one calculated from the optical model and the fluctuating matrix element is expressible as the sum of the Breit-Wigner amplitudes corresponding to each state in the compound nucleus. The measured cross-section is the sum of the direct and compound nucleus cross-sections

$$\frac{ds}{d\Omega} = \left(\frac{d\sigma}{d\Omega}\right)_{DI} + \left(\frac{d\sigma}{d\Omega}\right)_{CN} \qquad (3.60)$$

The direct interaction cross-section can be calculated for elastic scattering by the optical model and the compound nucleus cross-section may be calculated by the statistical theory.

CHAPTER 4

RESULTS AND DISCUSSION

4.1 Introduction

In this work it has been attempted to bring into focus the role physical pictures play in optical model of the nucleus by using the IAEA nuclear code 'SCAT 2' formally acquired under Computational Nuclear Physics programme of the IAEA TC project Mya/01/013 Applied Nuclear Physics and Nuclear Instrumentation.

These sources were checked and found to be compatible with Microsoft FORTRAN 5.0 and above, and have been compiled SCAT 2.for [14].

In this work we investigate the elastic cross-section dependence on target mass number using SCAT2 especially for 3-Li-7, 6-C-12, 12-Mg-24, 17-Cl-36, 20-Ca-40, 22-Ti-48, 26-Fe-56, 30-Zn-64, 32-Ge-72, 38-Sr-84, 42-Mo-96, 48-Cd-108, 50-Sn-120, 54-Xe-132, 60-Nd-144, 64-Gd-160, 72-Hf-180, 81-Tl-200, 90-Th-232 and 92-U-238, using SCAT2 and compare the results with those given in ENDF VI. We chose the targets to be light ones, intermediates ones and heavy ones so that the code may be valid for all kinds of nuclides. We see the results are quite the same and SCAT2 is found to be an efficient tool in studying nuclear cross-sections.

4.2 The Cross-sections Defined in SCAT2 Code

The calculation of cross-section is made on Transmission coefficients [9], which are defined as

$$T_{lj} = 1 - |\eta_{lj}|^2 \qquad (4.1)$$

and the scattering phase shift δ_{lj} is related to η_{lj} as $\eta_{lj} = \exp(2i\,\delta_{lj})$.

Thus the total cross-section is

$$\sigma_T = \frac{2\pi}{k^2}\sum_{l=0}^{\infty}\{(l+1)[1-R(\eta_l^+)]+l[1-R(\eta_l^-)]\} \qquad (4.2)$$

The elastic cross-section is

$$\sigma_E = \frac{\pi}{k^2}\sum_{\ell=0}^{\infty}\left[\left(\ell+1\left|1-\eta_\ell^+\right|^2+\ell\left|1-\eta_\ell^-\right|^2\right)\right] \qquad (4.3)$$

the reaction cross-section is

$$\sigma_R = \frac{\pi}{k}\sum_{\ell=0}^{\infty}\left[(\ell+1)T_\ell^+ + \ell T_\ell^-\right] \qquad (4.4)$$

4.3 Calculation Procedure

As the SCAT2 run under DOS, we have to load the DOS. After loading DOS, we have to load the SCAT2 program. Under SCAT2 program we open INPUT DAT and make some changes to input data file [8].

C:\>SCAT2>EDIT INPUT↵

The file is safe and closed. The calculation is done when we type this command.

C:\>SCAT2>SCAT2↵

To see and edit output results, we open SCAT2 and rename it.

C:\>SCAT2>EDIT OUTPUT↵

4.4 Results and Discussion

The elastic cross-sections dependence of target mass number at 0.0001 MeV is given in table 4.1 and fig (4.1). From the graph we can see the cross-sections are high at about mass numbers 12, 50 and 160.

The elastic cross-sections dependence of target mass number at 0.0002 MeV is given in table 4.2 and fig (4.2). From the graph we can see the cross-sections are high at about mass numbers 12, 50 and 160.

The elastic cross-sections dependence of target mass number at 0.0003 MeV is given in table 4.3 and fig (4.3). From the graph we can see the cross-sections are high at about mass numbers 12, 50 and 160.

The elastic cross-sections dependence of target mass number at 0.0004 MeV is given in table 4.4 and fig (4.4). From the graph we can see the cross-sections are high at about mass numbers 12, 50 and 160.

The elastic cross-sections dependence of target mass number at 0.0005 MeV is given in table 4.5 and fig (4.5). From the graph we can see the cross-sections are high at about mass numbers 12, 50 and 160.

The elastic cross-sections dependence of target mass number at 0.0006 MeV is given in table 4.6 and fig (4.6). From the graph we can see the cross-sections are high at about mass numbers 12, 50 and 160.

The elastic cross-sections dependence of target mass number at 0.0007 MeV is given in table 4.7 and fig (4.7). From the graph we can see the cross-sections are high at about mass numbers 12, 50 and 160.

The elastic cross-sections dependence of target mass number at 0.0008 MeV is given in table 4.8 and fig (4.8). From the graph we can see the cross-sections are high at about mass numbers 12, 50 and 160.

The elastic cross-sections dependence of target mass number at 0.0009 MeV is given in table 4.9 and fig (4.9). From the graph we can see the cross-sections are high at about mass numbers 12, 50 and 160.

The elastic cross-sections dependence of target mass number at 0.0010 MeV is given in table 4.10 and fig (4.10). From the graph we can see the cross-sections are high at about mass numbers 12, 50 and 160.

The elastic cross-sections dependence of target mass number at 0.005 MeV is given in table 4.11 and fig (4.11). From the graph we can see the cross-sections are high at about mass numbers 12, 50 and 160.

The elastic cross-sections dependence of target mass number at 0.045 MeV is given in table 4.12 and fig (4.12). From the graph we can see the cross-sections are high at about mass numbers 12, 50 and 160.

The elastic cross-sections dependence of target mass number at 0.085 MeV is given in table 4.13 and fig (4.13). From the graph we can see the cross-sections seem to increase with mass numbers.

The elastic cross-sections dependence of target mass number at 0.125 MeV is given in table 4.14 and fig (4.14). From the graph we can see the cross-sections seem to increase with mass numbers.

The elastic cross-sections dependence of target mass number at 0.165 MeV is given in table 4.15 and fig (4.15). From the graph we can see the cross-sections seem to increase with mass numbers.

The elastic cross-sections dependence of target mass number at 0.205 MeV is given in table 4.16 and fig (4.16). From the graph we can see the cross-sections seem to increase with mass numbers.

The elastic cross-sections dependence of target mass number at 0.245 MeV is given in table 4.17 and fig (4.17). From the graph we can see the cross-sections seem to increase with mass numbers.

The elastic cross-sections dependence of target mass number at 0.285 MeV is given in table 4.18 and fig (4.18). From the graph we can see the cross-sections seem to increase with mass numbers.

The elastic cross-sections dependence of target mass number at 0.325 MeV is given in table 4.19 and fig (4.19). From the graph we can see the cross-sections seem to increase with mass numbers.

The elastic cross-sections dependence of target mass number at 0.365 MeV is given in table 4.20 and fig (4.20). From the graph we can see the cross-sections seem to increase with mass numbers.

The elastic cross-sections dependence of target mass number at 0.405 MeV is given in table 4.21 and fig (4.21). From the graph we can see the cross-sections seem to increase with mass numbers.

The elastic cross-sections dependence of target mass number at 0.445 MeV is given in table 4.22 and fig (4.22). From the graph we can see the cross-sections seem to increase with mass numbers.

The elastic cross-sections dependence of target mass number at 0.485 MeV is given in table 4.23 and fig (4.23). From the graph we can see the cross-sections seem to increase with mass numbers.

The elastic cross-sections dependence of target mass number at 1 MeV is given in table 4.24 and fig (4.24). From the graph we can see the cross-sections seem to increase with mass numbers.

The elastic cross-sections dependence of target mass number at 2 MeV is given in table 4.25 and fig (4.25). From the graph we can see the cross-sections seem to increase with mass numbers.

The elastic cross-sections dependence of target mass number at 3 MeV is given in table 4.26 and fig (4.26). From the graph we can see the cross-sections seem to increase with mass numbers.

The elastic cross-sections dependence of target mass number at 4 MeV is given in table 4.27 and fig (4.27). From the graph we can see the cross-sections seem to increase with mass numbers.

The elastic cross-sections dependence of target mass number at 5 MeV is given in table 4.28 and fig (4.28). From the graph we can see the cross-sections increase with mass numbers.

The elastic cross-sections dependence of target mass number at 6 MeV is given in table 4.29 and fig (4.29). From the graph we can see the cross-sections increase with mass numbers.

The elastic cross-sections dependence of target mass number at 7 MeV is given in table 4.30 and fig (4.30). From the graph we can see the cross-sections increase with mass numbers.

The elastic cross-sections dependence of target mass number at 8 MeV is given in table 4.31 and fig (4.31). From the graph we can see the cross-sections increase with mass numbers.

The elastic cross-sections dependence of target mass number at 9 MeV is given in table 4.32 and fig (4.32). From the graph we can see the cross-sections increase with mass numbers.

The elastic cross-sections dependence of target mass number at 10 MeV is given in table 4.33 and fig (4.33). From the graph we can see the cross-sections increase with mass numbers.

The comparison of elastic cross-sections obtained by SCAT2 and those given in ENDF file [14] are shown in table (4.34), table (4.35), fig (4.34) and fig (4.35), and we find the results are quite the same.

Table (4.1) Elastic Scattering CS at 0.0001 MeV for Various Targets

Target	A (amu)	Elastic CS(B)
3-Li	7	0.5734
6-C	12	5.0842
12-Mg	24	2.6477
17-Cl	36	1.6620
20-Ca	40	1.5672
22-Ti	48	4.6380
26-Fe	56	8.4795
30-Zn	64	7.7082
32-Ge	72	6.8154
38-Sr	84	5.9588
42-Mo	96	5.3429
48-Cd	108	4.7574
50-Sn	120	4.1284
54-Xe	132	3.6680
60-Nd	144	4.8732
64-Gd	160	11.4453
72-Hf	180	12.4267
81-Tl	200	11.2840
90-Th	232	9.8032
92-U	238	9.6191

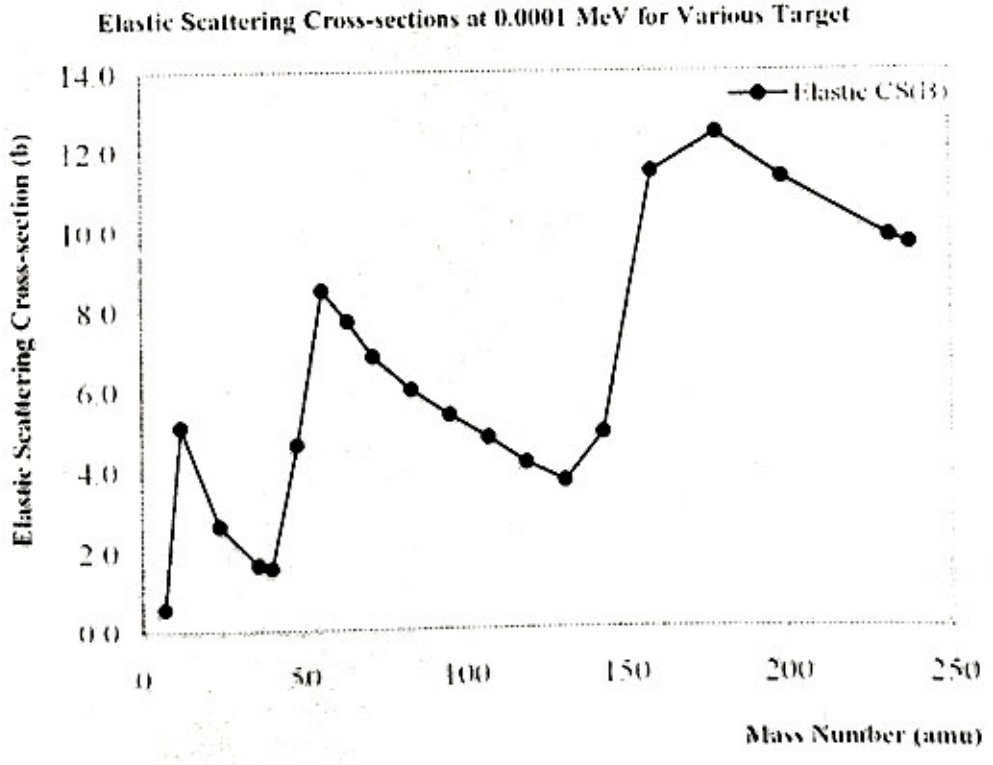

Fig (4.1) Elastic Scattering CS dependance of Mass Number at 0.0001 MeV

Table (4.2) **Elastic Scattering CS at 0.0002 MeV for Various Targets**

Target	A (amu)	Elastic CS(B)
3-Li	7	0.5715
6-C	12	5.0562
12-Mg	24	2.6441
17-Cl	36	1.6585
20-Ca	40	1.5619
22-Ti	48	4.5992
26-Fe	56	8.4215
30-Zn	64	7.6795
32-Ge	72	6.7989
38-Sr	84	5.949
42-Mo	96	5.3353
48-Cd	108	4.7504
50-Sn	120	4.1202
54-Xe	132	3.6557
60-Nd	144	4.8413
64-Gd	160	11.3461
72-Hf	180	12.3724
81-Tl	200	11.1004
90-Th	232	9.7916
92-U	238	9.6043

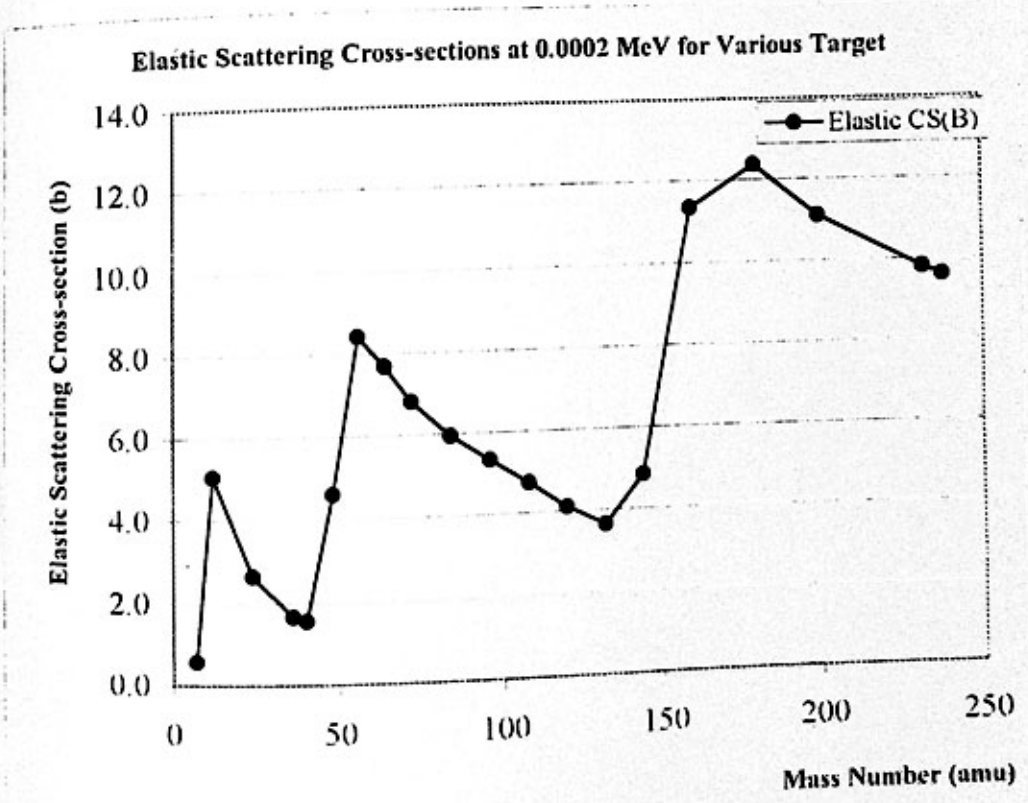

Fig (4.2) Elastic Scattering CS dependance of Mass Number at 0.0002 MeV

Table (4.3) Elastic Scattering CS at 0.0003 MeV for Various Targets

Target	A (amu)	Elastic CS(B)
3-Li	7	0.5701
6-C	12	5.0347
12-Mg	24	2.6413
17-Cl	36	1.6558
20-Ca	40	1.5579
22-Ti	48	4.5697
26-Fe	56	8.3771
30-Zn	64	7.6573
32-Ge	72	6.7861
38-Sr	84	5.9414
42-Mo	96	5.3294
48-Cd	108	4.7449
50-Sn	120	4.1139
54-Xe	132	3.6462
60-Nd	144	4.8169
64-Gd	160	11.2706
72-Hf	180	12.3305
81-Tl	200	11.0786
90-Th	232	9.7792
92-U	238	9.5926

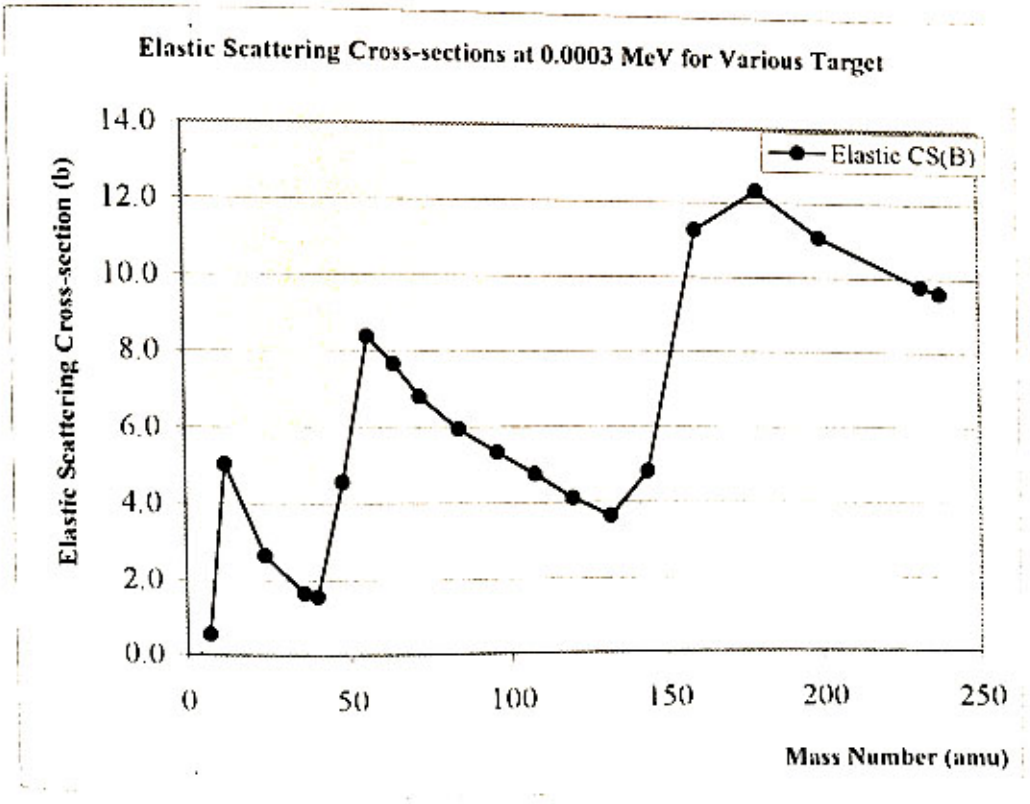

Fig (4.3) Elastic Scattering CS dependance of Mass Number at 0.0003 MeV

Table (4.4) Elastic Scattering CS at 0.0004 MeV for Various Targets

Target	A (amu)	Elastic CS(B)
3-Li	7	0.5688
6-C	12	5.0167
12-Mg	24	2.639
17-Cl	36	1.6535
20-Ca	40	1.5545
22-Ti	48	4.545
26-Fe	56	8.3398
30-Zn	64	7.6386
32-Ge	72	6.7753
38-Sr	84	5.9349
42-Mo	96	5.3244
48-Cd	108	4.7402
50-Sn	120	4.1086
54-Xe	132	3.6382
60-Nd	144	4.7963
64-Gd	160	11.2072
72-Hf	180	12.295
81-Tl	200	11.06
90-Th	232	9.7686
92-U	238	9.5826

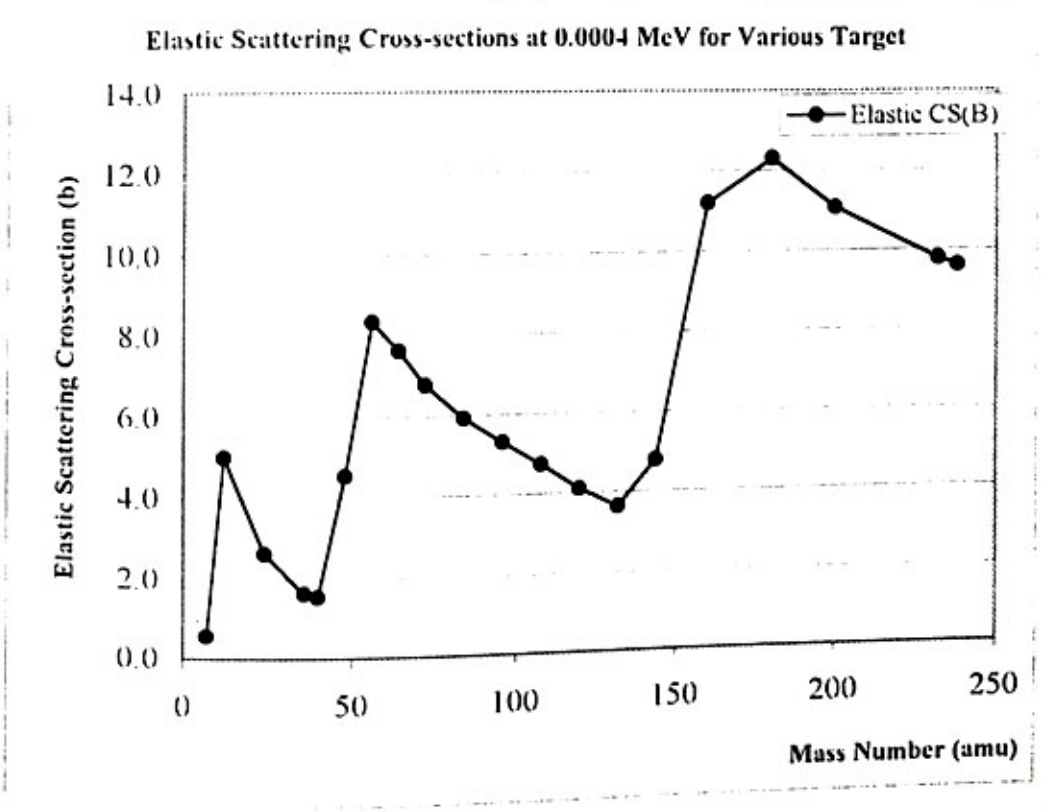

Fig (4.4) Elastic Scattering CS dependance of Mass Number at 0.0004 MeV

Table (4.5) Elastic Scattering CS at 0.0005 MeV for Various Targets

Target	A (amu)	Elastic CS(B)
3-Li	7	0.5677
6-C	12	5.0009
12-Mg	24	2.6369
17-Cl	36	1.6515
20-Ca	40	1.5516
22-Ti	48	4.5233
26-Fe	56	8.3071
30-Zn	64	7.622
32-Ge	72	6.7658
38-Sr	84	5.929
42-Mo	96	5.32
48-Cd	108	4.736
50-Sn	120	4.1039
54-Xe	132	3.6312
60-Nd	144	4.7788
64-Gd	160	11.1515
72-Hf	180	12.2637
81-Tl	200	11.0435
90-Th	232	9.7591
92-U	238	9.5737

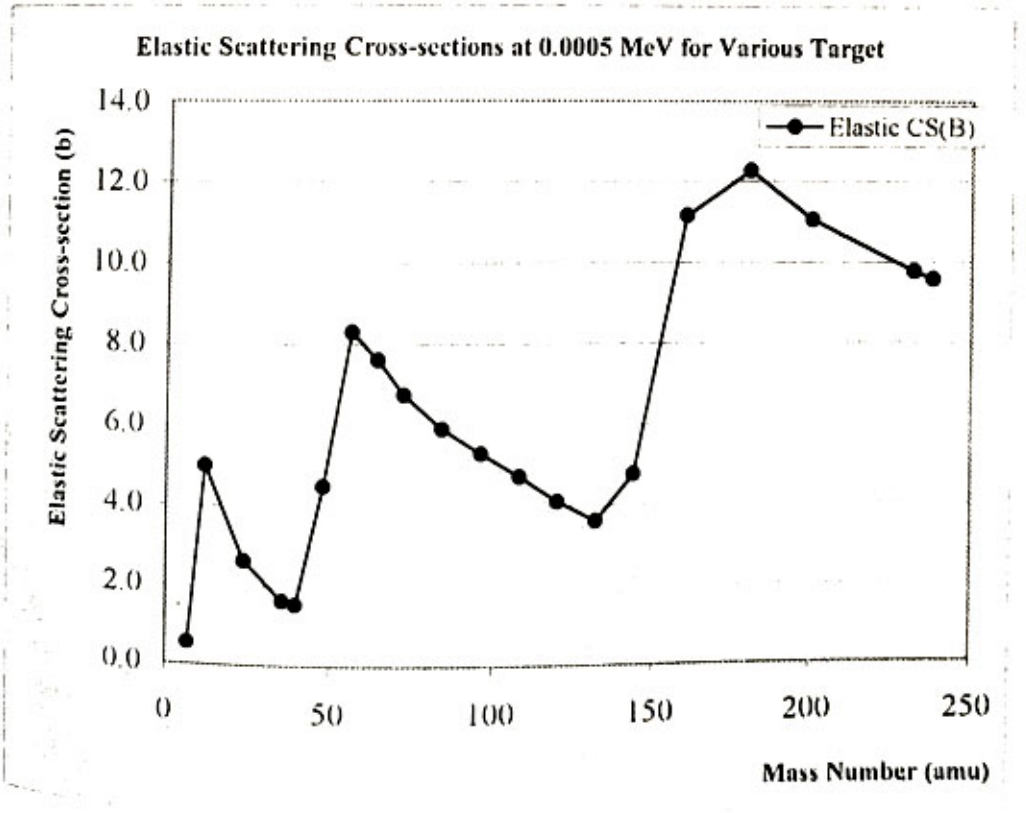

Fig (4.5) Elastic Scattering CS dependance of Mass Number at 0.0005 MeV

Table (4.6) **Elastic Scattering CS at 0.0006 MeV for Various Targets**

Target	A (amu)	Elastic CS(B)
3-Li	7	0.5667
6-C	12	4.9866
12-Mg	24	2.635
17-Cl	36	1.6497
20-Ca	40	1.5489
22-Ti	48	4.5038
26-Fe	56	8.2776
30-Zn	64	7.607
32-Ge	72	6.757
38-Sr	84	5.9238
42-Mo	96	5.3159
48-Cd	108	4.7323
50-Sn	120	4.0996
54-Xe	132	3.6248
60-Nd	144	4.7621
64-Gd	160	11.1014
72-Hf	180	12.2352
81-Tl	200	11.0284
90-Th	232	9.7504
92-U	238	9.5655

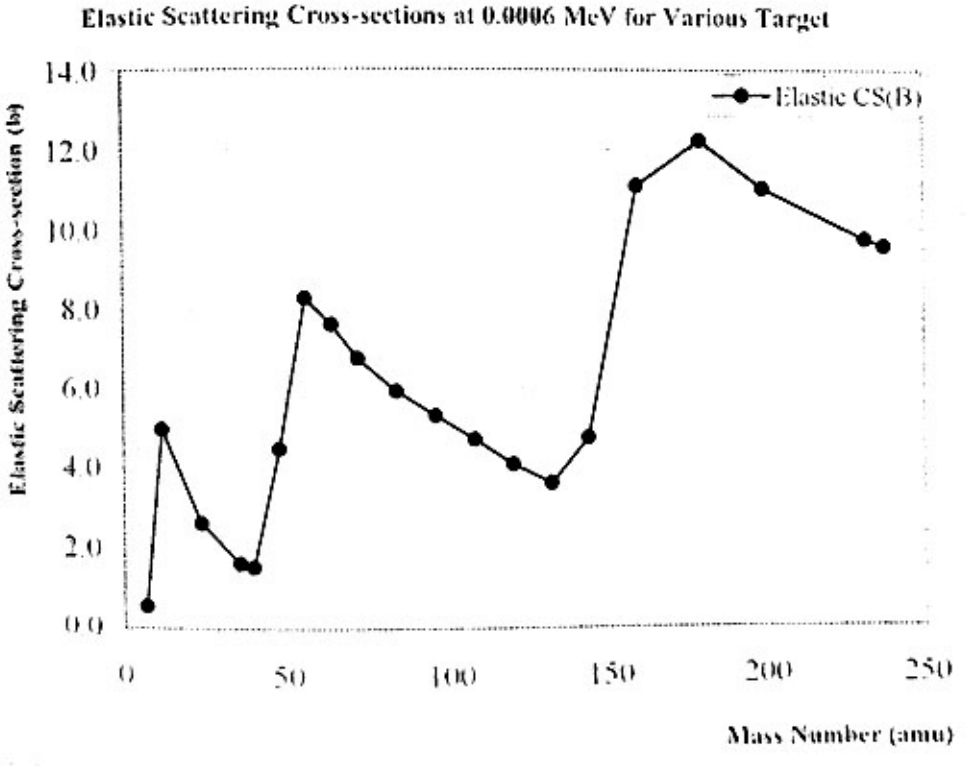

Fig (4.6) Elastic Scattering CS dependance of Mass Number at 0.0006 MeV

Table (4.7) Elastic Scattering CS at 0.0007 MeV for Various Targets

Target	A (amu)	Elastic CS(B)
3-Li	7	0.5658
6-C	12	4.9735
12-Mg	24	2.6333
17-Cl	36	1.648
20-Ca	40	1.5464
22-Ti	48	4.486
26-Fe	56	8.2505
30-Zn	64	7.5932
32-Ge	72	6.949
38-Sr	84	5.9189
42-Mo	96	5.3122
48-Cd	108	4.7288
50-Sn	120	4.0957
54-Xe	132	3.6189
60-Nd	144	4.7471
64-Gd	160	11.0555
72-Hf	180	12.2089
81-Tl	200	11.0145
90-Th	232	9.7423
92-U	238	9.5579

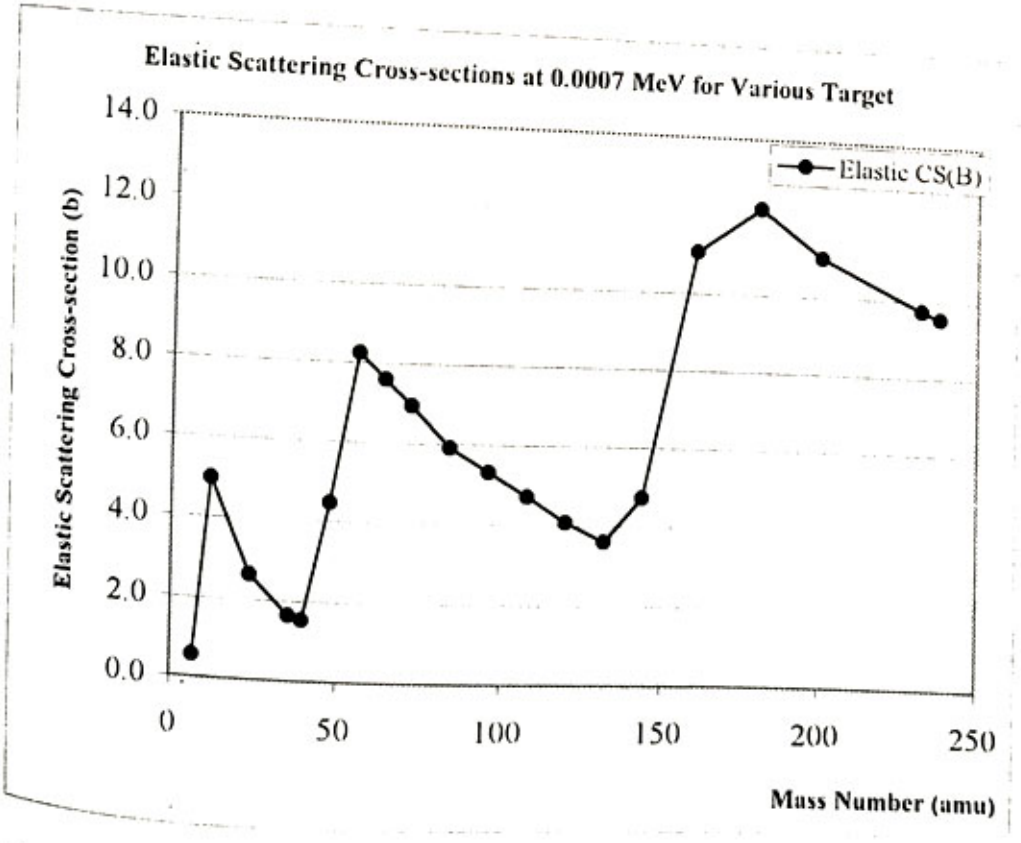

Fig (4.7) Elastic Scattering CS dependance of Mass Number at 0.0007 MeV

Table (4.8) Elastic Scattering CS at 0.0008 MeV for Various Targets

Target	A (amu)	Elastic CS(B)
3-Li	7	0.5649
6-C	12	4.9614
12-Mg	24	2.6317
17-Cl	36	1.6464
20-Ca	40	1.5441
22-Ti	48	4.4694
26-Fe	56	8.2254
30-Zn	64	7.5803
32-Ge	72	6.7415
38-Sr	84	5.9144
42-Mo	96	5.3087
48-Cd	108	4.7256
50-Sn	120	4.092
54-Xe	132	3.6135
60-Nd	144	4.7338
64-Gd	160	11.0129
72-Hf	180	12.1844
81-Tl	200	11.0014
90-Th	232	9.7347
92-U	238	9.5507

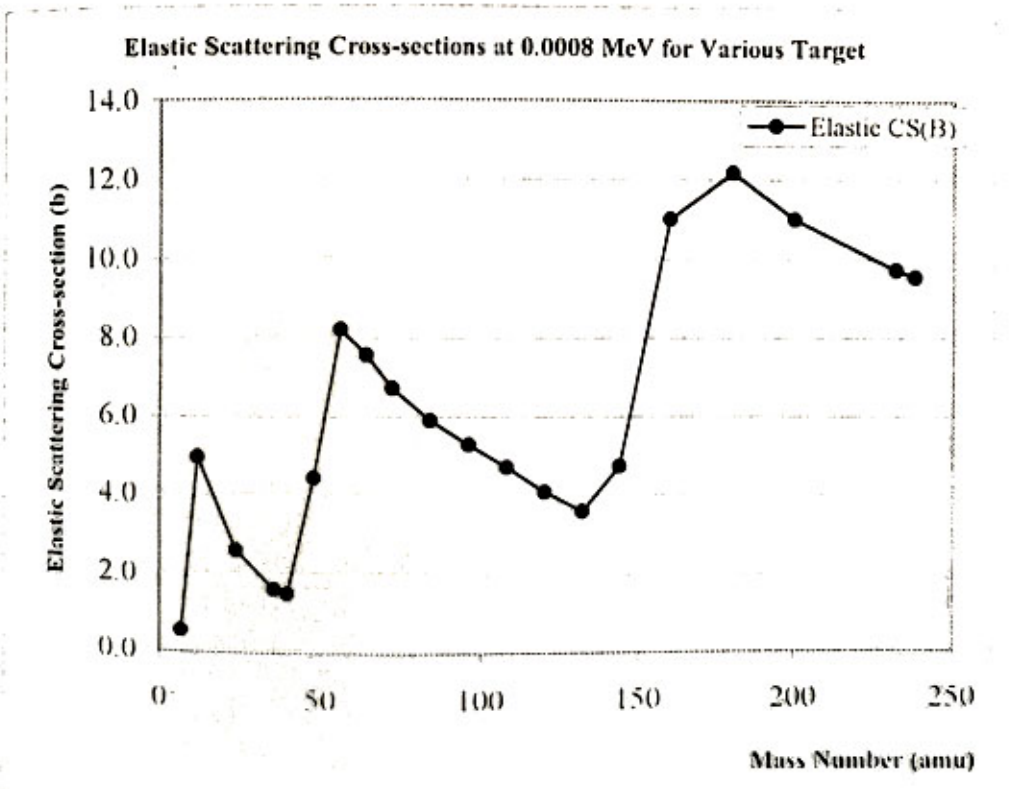

Fig (4.8) Elastic Scattering CS dependance of Mass Number at 0.0008 MeV

Table (4.9) Elastic Scattering CS at 0.0009 MeV for Various Targets

Target	A (amu)	Elastic CS(B)
3-Li	7	0.5642
6-C	12	4.95
12-Mg	24	2.6301
17-Cl	36	1.6449
20-Ca	40	1.5419
22-Ti	48	4.454
26-Fe	56	8 2018
30-Zn	64	7.5682
32-Ge	72	6.7344
38-Sr	84	5.9101
42-Mo	96	5.3054
48-Cd	108	4.7225
50-Sn	120	4.0585
54-Xe	132	3.6083
60-Nd	144	4.7203
64-Gd	160	10.973
72-Hf	180	12.1613
81-Tl	200	10.989
90-Th	232	9.7275
92-U	238	9.5439

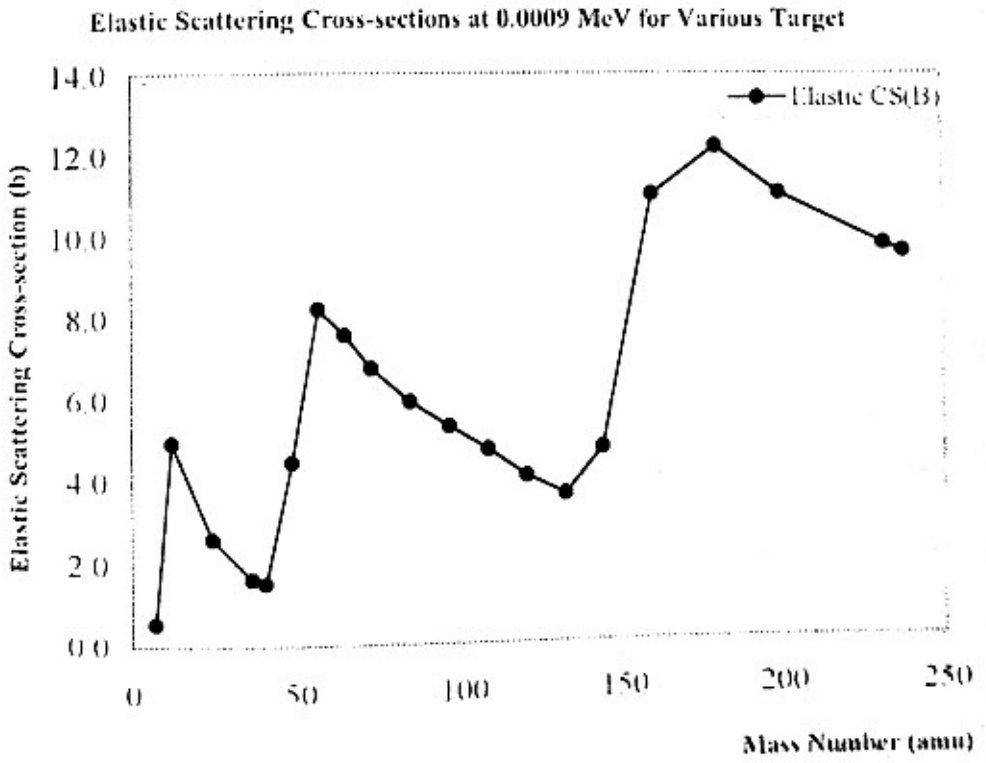

Fig (4 9) Elastic Scattering CS dependance of Mass Number at 0 0009 MeV

Table (4.10) Elastic Scattering CS at 0.001 MeV for Various Targets

Target	A (amu)	Elastic CS(B)
3-Li	7	0.5634
6-C	12	4.9392
12-Mg	24	2.6287
17-Cl	36	1.6436
20-Ca	40	1.5399
22-Ti	48	4.4394
26-Fe	56	8.1795
30-Zn	64	7.5567
32-Ge	72	6.7277
38-Sr	84	5.906
42-Mo	96	5.3022
48-Cd	108	4.7196
50-Sn	120	4.0852
54-Xe	132	3.6035
60-Nd	144	4.708
64-Gd	160	10.9354
72-Hf	180	12.1395
81-Tl	200	10.9772
90-Th	232	9.7206
92-U	238	9.5374

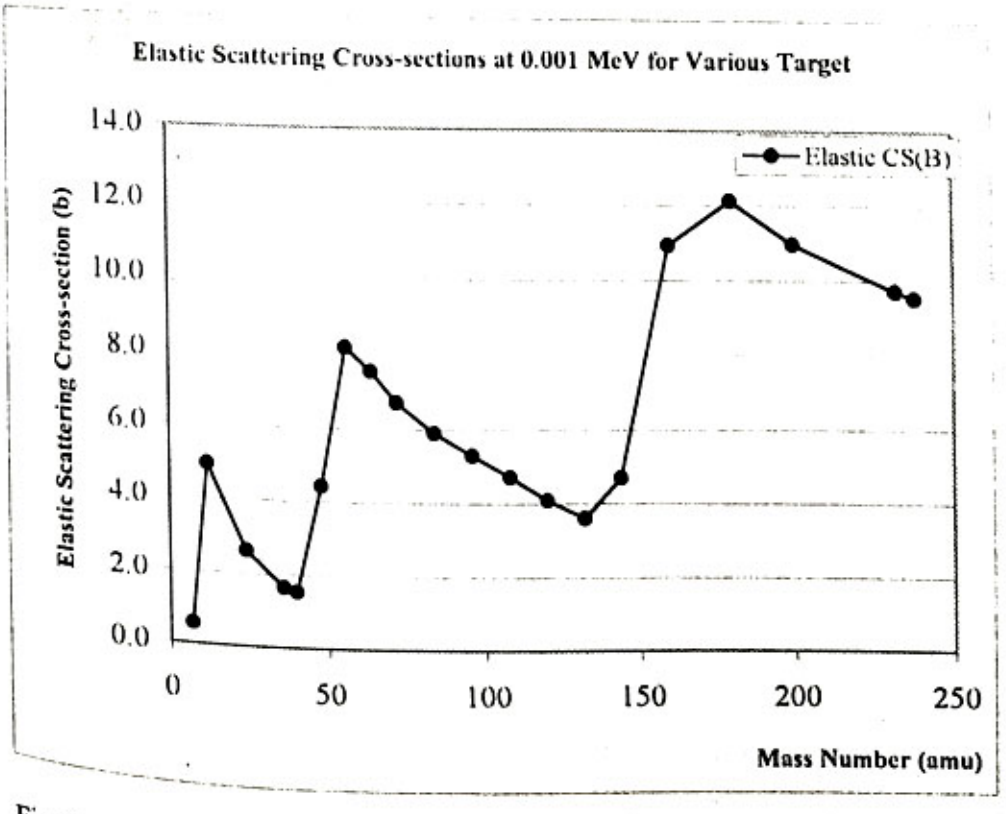

Fig (4.10) Elastic Scattering CS dependance of Mass Number at 0.001 MeV

Table (4.11) Elastic Scattering CS at 0.005 MeV for Various Targets

Target	A (amu)	Elastic CS(B)
3-Li	7	0.5454
6-C	12	2.6857
12-Mg	24	2.5927
17-Cl	36	1.6092
20-Ca	40	1.4908
22-Ti	48	4.1025
26-Fe	56	7.6567
30-Zn	64	7.2760
32-Ge	72	6.6590
38-Sr	84	5.8012
42-Mo	96	5.2215
48-Cd	108	4.6459
50-Sn	120	4.0039
54-Xe	132	3.4864
60-Nd	144	4.4192
64-Gd	160	10.0600
72-Hf	180	11.5989
81-Tl	200	10.6739
90-Th	232	9.5379
92-U	238	9.3652

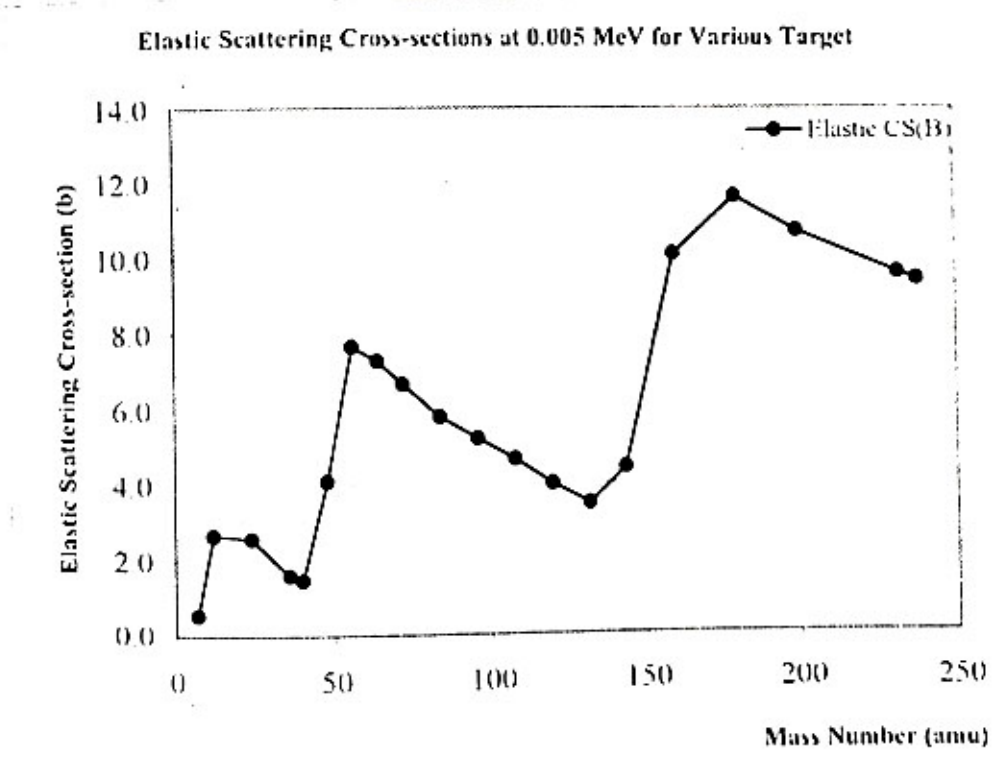

Fig (4.11) Elastic Scattering CS dependance of Mass Number at 0 005 MeV

Table (4.12) Elastic Scattering CS at 0.045 MeV for Various Targets

Target	A (amu)	Elastic CS(B)
3-Li	7	0.4816
6-C	12	3.8578
12-Mg	24	2.4525
17-Cl	36	1.4951
20-Ca	40	1.3256
22-Ti	48	3.0883
26-Fe	56	5.9703
30-Zn	64	6.2171
32-Ge	72	5.861
38-Sr	84	5.346
42-Mo	96	4.9052
48-Cd	108	4.3848
50-Sn	120	3.726
54-Xe	132	3.1006
60-Nd	144	3.5076
64-Gd	160	7.3609
72-Hf	180	9.5209
81-Tl	200	9.3235
90-Th	232	8.6941
92-U	238	8.5977

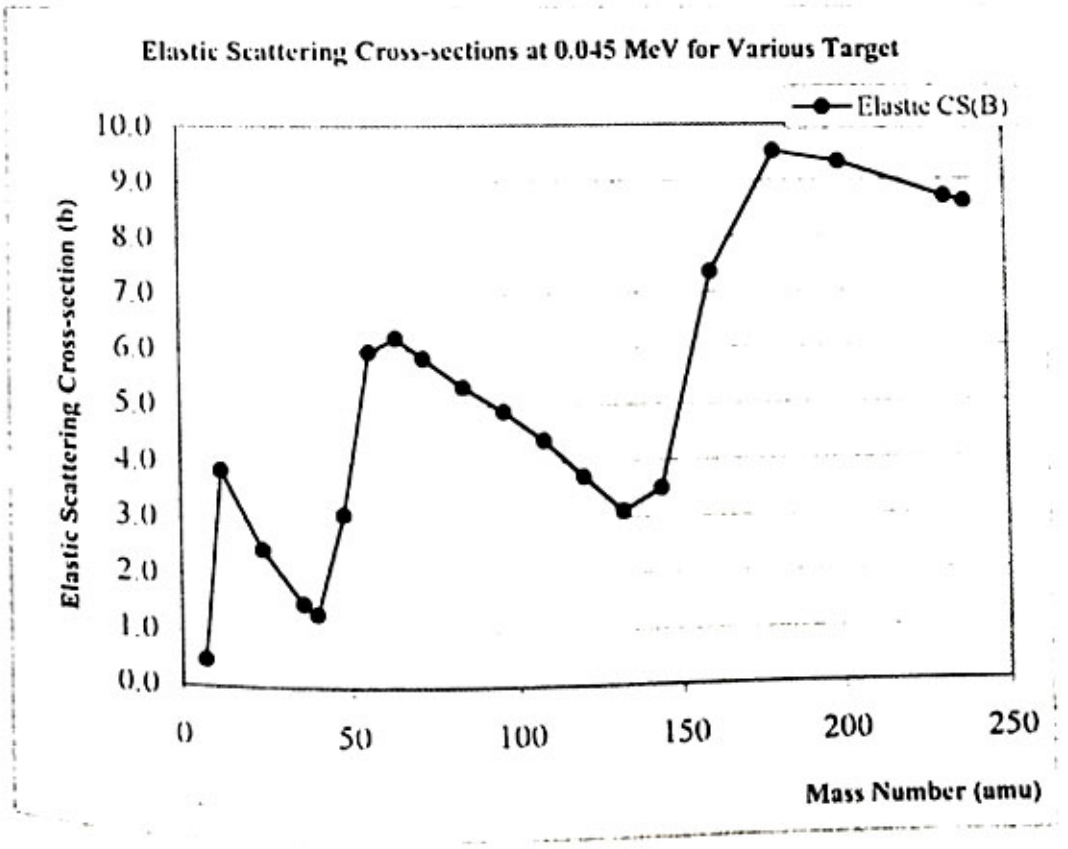

Fig (4.12) Elastic Scattering CS dependance of Mass Number at 0.045 MeV

Table (4.13) **Elastic Scattering CS at 0.085 MeV for Various Targets**

Target	A (amu)	Elastic CS(B)
3-Li	7	0.4482
6-C	12	3.4508
12-Mg	24	2.3778
17-Cl	36	1.4466
20-Ca	40	1.2509
22-Ti	48	2.6391
26-Fe	56	5.1607
30-Zn	64	5.6189
32-Ge	72	5.4296
38-Sr	84	5.0651
42-Mo	96	4.7699
48-Cd	108	4.3052
50-Sn	120	3.6343
54-Xe	132	2.955
60-Nd	144	3.1204
64-Gd	160	6.1574
72-Hf	180	8.3609
81-Tl	200	8.4611
90-Th	232	8.1938
92-U	238	8.1865

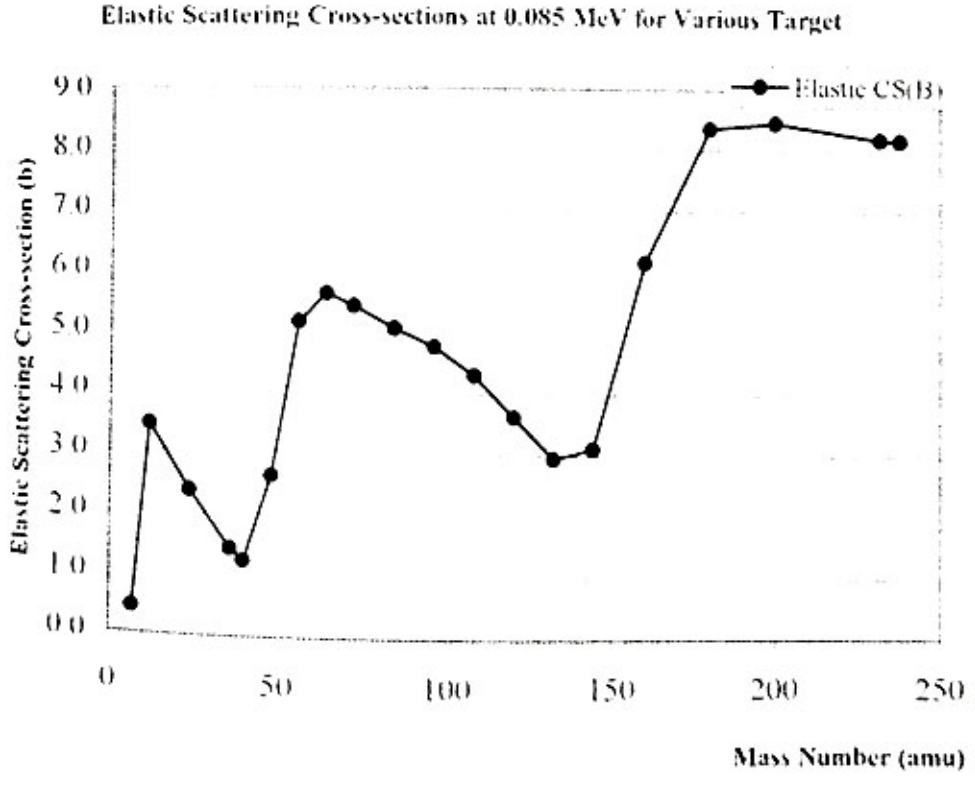

Fig (4.13) Elastic Scattering CS dependance of Mass Number at 0.085 MeV

Table (4.14) Elastic Scattering CS at 0.125 MeV for Various Targets

Target	A (amu)	Elastic CS(B)
3-Li	7	0.4239
6-C	12	3.1597
12-Mg	24	2.3287
17-Cl	36	1.4228
20-Ca	40	1.2069
22-Ti	48	2.3414
26-Fe	56	4.5949
30-Zn	64	5.1625
32-Ge	72	5.0844
38-Sr	84	4.8483
42-Mo	96	4.7073
48-Cd	108	4.296
50-Sn	120	3.6134
54-Xe	132	2.8946
60-Nd	144	2.8939
64-Gd	160	5.3706
72-Hf	180	7.501
81-Tl	200	7.7731
90-Th	232	7.8253
92-U	238	7.9072

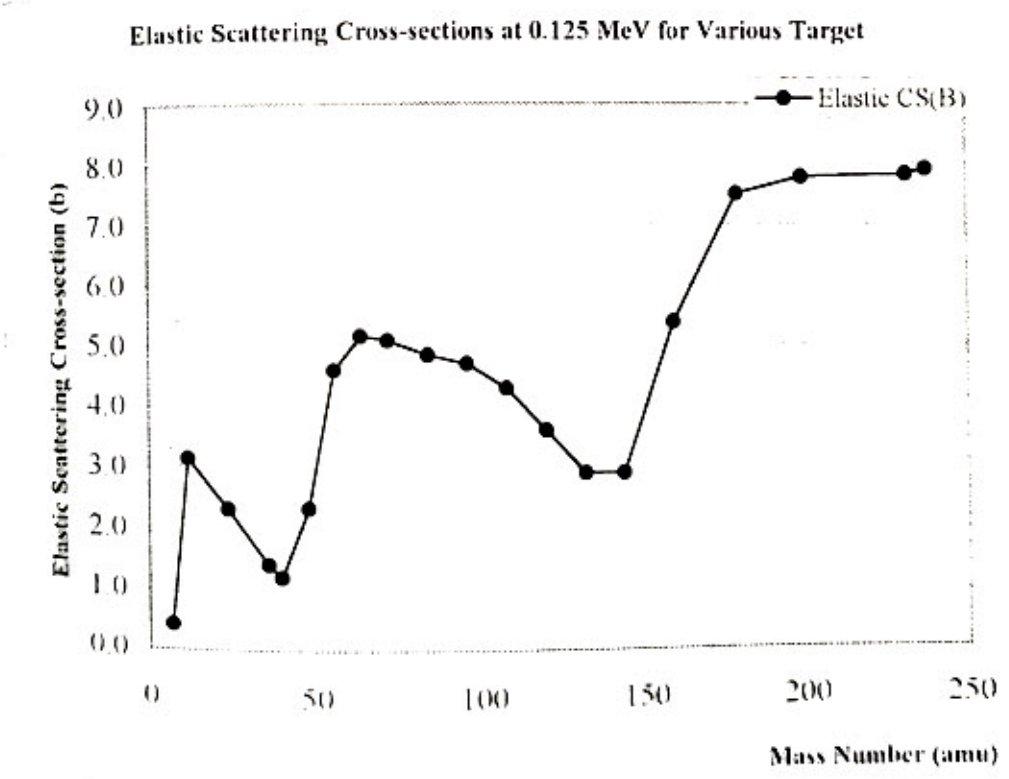

Fig (4.14) Elastic Scattering CS dependance of Mass Number at 0.125 MeV

Table (4.15) Elastic Scattering CS at 0.165 MeV for Various Targets

Target	A (amu)	Elastic CS(B)
3-Li	7	0.405
6-C	12	2.93
12-Mg	24	2.2961
17-Cl	36	1.4141
20-Ca	40	1.1812
22-Ti	48	2.1225
26-Fe	56	4.1587
30-Zn	64	4.7872
32-Ge	72	4.7904
38-Sr	84	4.6709
42-Mo	96	4.6819
48-Cd	108	4.3209
50-Sn	120	3.6302
54-Xe	132	2.8814
60-Nd	144	2.7552
64-Gd	160	4.8045
72-Hf	180	6.8174
81-Tl	200	7.1941
90-Th	232	7.5264
92-U	238	7.6888

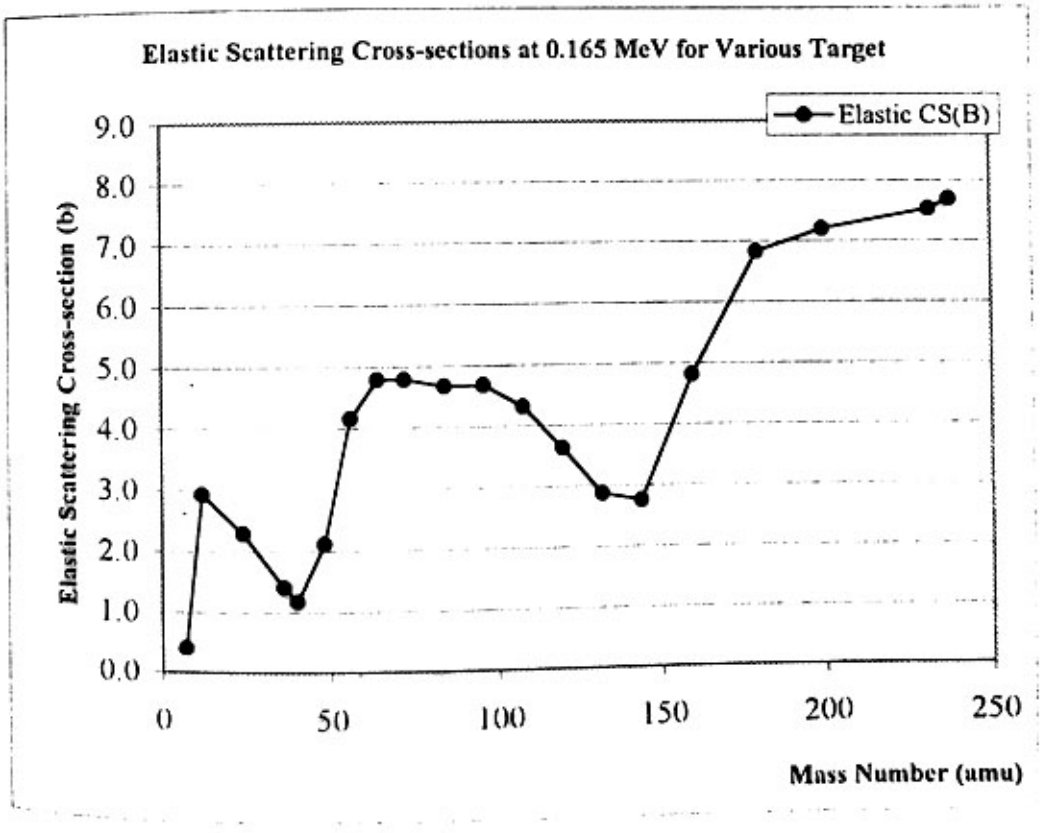

Fig (4.15) Elastic Scattering CS dependance of Mass Number at 0.165 MeV

Table (4.16) **Elastic Scattering CS at 0.205 MeV for Various Targets**

Target	A (amu)	Elastic CS(B)
3-Li	7	0.3898
6-C	12	2.7395
12-Mg	24	2.2752
17-Cl	36	1.4156
20-Ca	40	1.1677
22-Ti	48	1.9535
26-Fe	56	3.8057
30-Zn	64	4.467
32-Ge	72	4.5323
38-Sr	84	4.5204
42-Mo	96	4.6743
48-Cd	108	4.361
50-Sn	120	3.6674
54-Xe	132	2.8967
60-Nd	144	2.672
64-Gd	160	4.3788
72-Hf	180	6.2556
81-Tl	200	6.6943
90-Th	232	7.2662
92-U	238	7.497

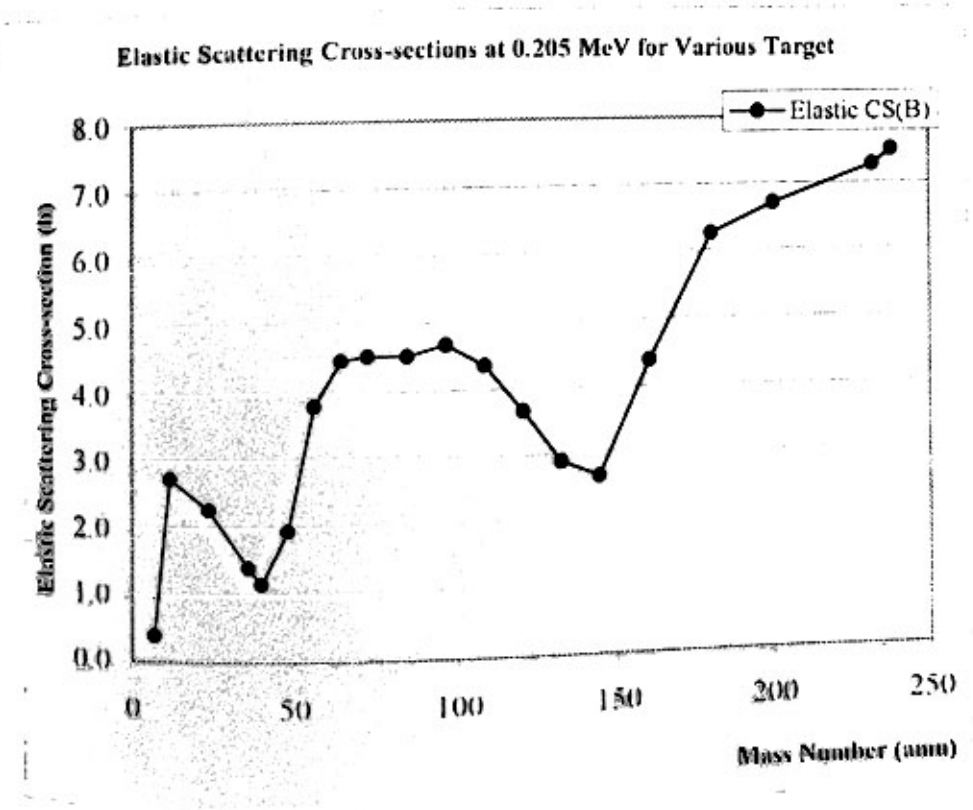

Fig.(4.16) Elastic Scattering CS dependance of Mass Number at 0.205 MeV

Table (4.17) **Elastic Scattering CS at 0.245 MeV for Various Targets**

Target	A (amu)	Elastic CS(B)
3-Li	7	0.3774
6-C	12	2.5766
12-Mg	24	2.2629
17-Cl	36	1.4241
20-Ca	40	1.1631
22-Ti	48	1.8191
26-Fe	56	3.5117
30-Zn	64	4.1879
32-Ge	72	4.3018
38-Sr	84	4.389
42-Mo	96	4.6732
48-Cd	108	4.4058
50-Sn	120	3.715
54-Xe	132	2.9297
60-Nd	144	2.6265
64-Gd	160	4.051
72-Hf	180	5.785
81-Tl	200	6.2561
90-Th	232	7.0278
92-U	238	7.3149

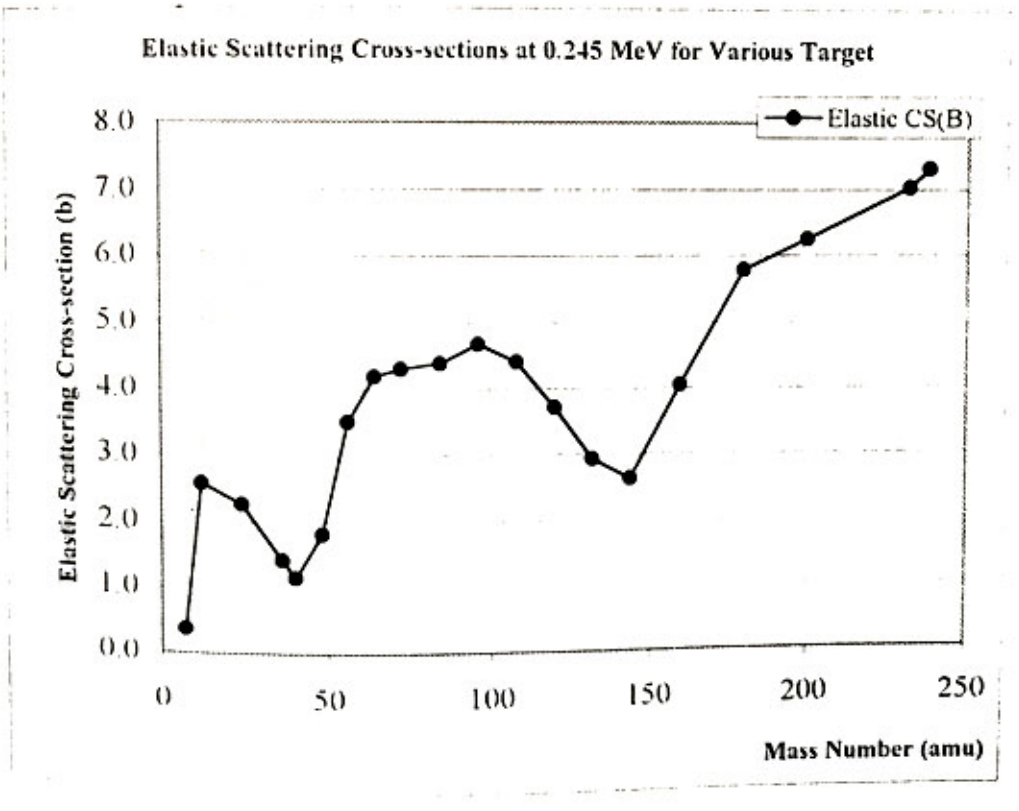

Fig (4.17) Elastic Scattering CS dependance of Mass Number at 0.245 MeV

Table (4.18) **Elastic Scattering CS at 0.285 MeV for Various Targets**

Target	A (amu)	Elastic CS(B)
3-Li	7	0.3671
6-C	12	2.4345
12-Mg	24	2.2567
17-Cl	36	1.4376
20-Ca	40	1.165
22-Ti	48	1.7103
26-Fe	56	3.2019
30-Zn	64	3.9412
32-Ge	72	4.0934
38-Sr	84	4.2715
42-Mo	96	4.672
48-Cd	108	4.4495
50-Sn	120	3.767
54-Xe	132	2.9734
60-Nd	144	2.6078
64-Gd	160	3.7959
72-Hf	180	5.3863
81-Tl	200	5.8685
90-Th	232	6.8024
92-U	238	7.1347

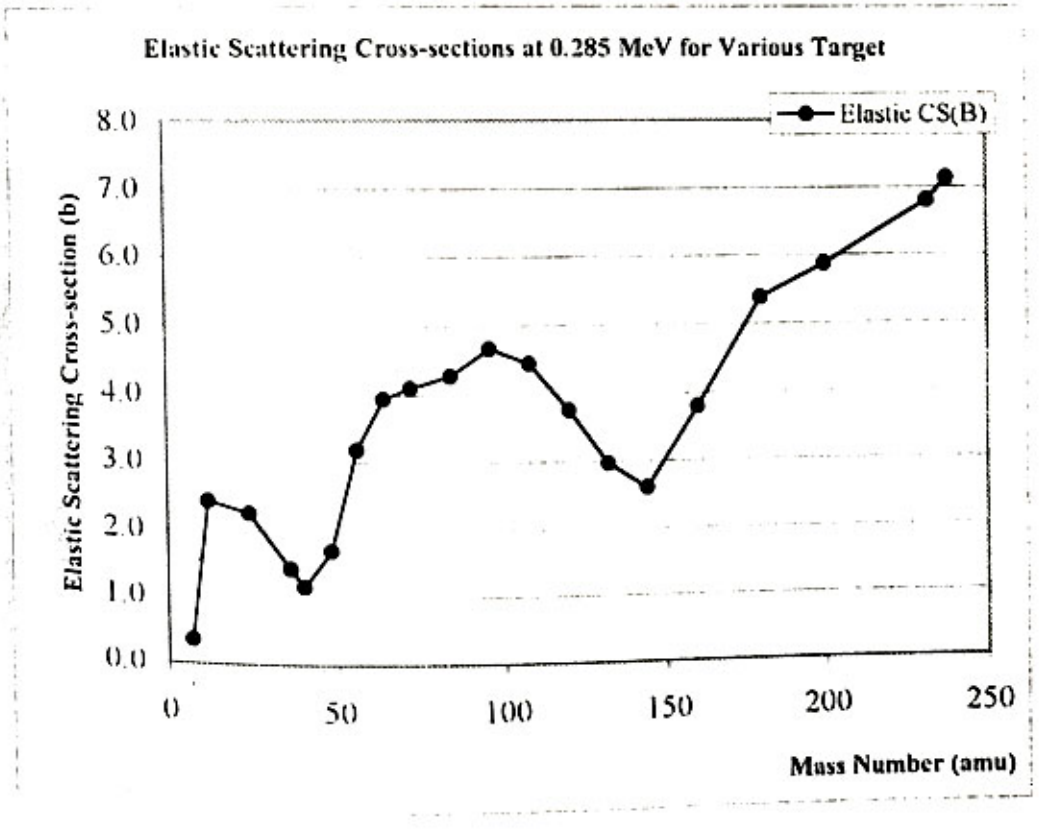

Fig (4.18) Elastic Scattering CS dependance of Mass Number at 0.285 MeV

Table (4.19) Elastic Scattering CS at 0.325 MeV for Various Targets

Target	A (amu)	Elastic CS(B)
3-Li	7	0.3586
6-C	12	2.3086
12-Mg	24	2.2548
17-Cl	36	1.4545
20-Ca	40	1.1718
22-Ti	48	1.6213
26-Fe	56	3.0967
30-Zn	64	3.7208
32-Ge	72	3.9034
38-Sr	84	4.1641
42-Mo	96	4.6672
48-Cd	108	4.4886
50-Sn	120	3.8193
54-Xe	132	3.0235
60-Nd	144	2.6088
64-Gd	160	3.5968
72-Hf	180	5.046
81-Tl	200	5.5233
90-Th	232	6.5854
92-U	238	6.9534

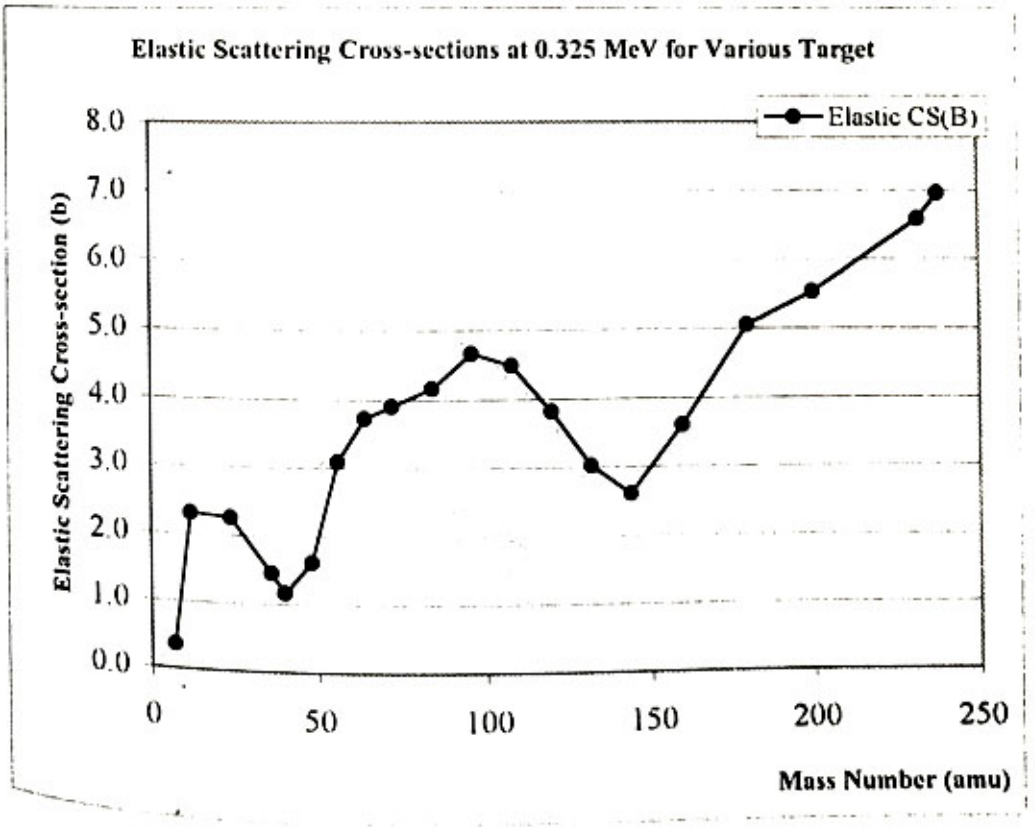

Fig (4.19) Elastic Scattering CS dependance of Mass Number at 0.325 MeV

Table (4.20) Elastic Scattering CS at 0.365 MeV for Various Targets

Target	A (amu)	Elastic CS(B)
3-Li	7	0.3516
6-C	12	2.1957
12-Mg	24	2.2558
17-Cl	36	1.4238
20-Ca	40	1.1823
22-Ti	48	1.5479
26-Fe	56	2.8596
30-Zn	64	3.5224
32-Ge	72	3.7291
38-Sr	84	4.0642
42-Mo	96	4.6569
48-Cd	108	4.5216
50-Sn	120	3.8698
54-Xe	132	3.0769
60-Nd	144	2.6246
64-Gd	160	3.4424
72-Hf	180	4.7545
81-Tl	200	5.2147
90-Th	232	6.3745
92-U	238	6.7701

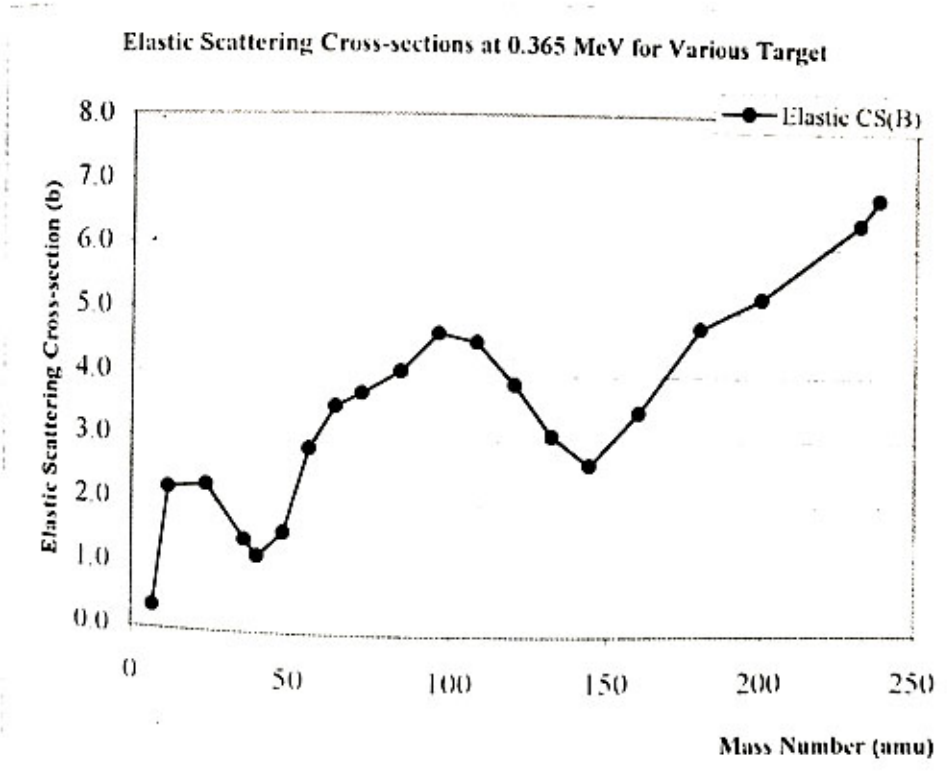

Fig (4.20) Elastic Scattering CS dependance of Mass Number at 0.365 MeV

Table (4.21) Elastic Scattering CS at 0.405 MeV for Various Targets

Target	A (amu)	Elastic CS(B)
3-Li	7	0.3459
6-C	12	2.0937
12-Mg	24	2.2586
17-Cl	36	1.4946
20-Ca	40	1.1955
22-Ti	48	1.4842
26-Fe	56	2.6956
30-Zn	64	3.3429
32-Ge	72	3.5683
38-Sr	84	3.9698
42-Mo	96	4.6403
48-Cd	108	4.5475
50-Sn	120	3.9169
54-Xe	132	3.1318
60-Nd	144	2.652
64-Gd	160	3.3242
72-Hf	180	4.5044
81-Tl	200	4.938
90-Th	232	6.169
92-U	238	6.5854

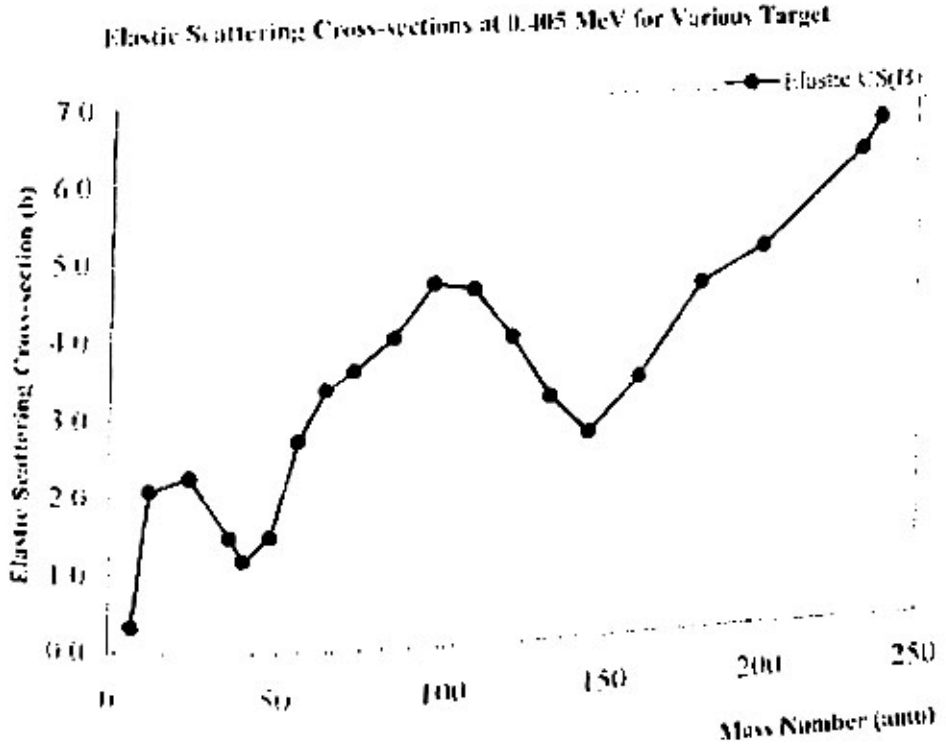

Fig (4.21) Elastic Scattering CS dependance of Mass Number at 0.405 MeV

Table (4.22) Elastic Scattering CS at 0.445 MeV for Various Targets

Target	A (amu)	Elastic CS(B)
3-Li	7	0.3412
6-C	12	2.0008
12-Mg	24	2.2623
17-Cl	36	1.5164
20-Ca	40	1.2108
22-Ti	48	1.4371
26-Fe	56	2.551
30-Zn	64	3.1797
32-Ge	72	3.4193
38-Sr	84	3.8796
42-Mo	96	4.6176
48-Cd	108	4.5663
50-Sn	120	3.9599
54-Xe	132	3.1868
60-Nd	144	2.6883
64-Gd	160	3.2359
72-Hf	180	4.2896
81-Tl	200	4.6895
90-Th	232	5.9687
92-U	238	6.4002

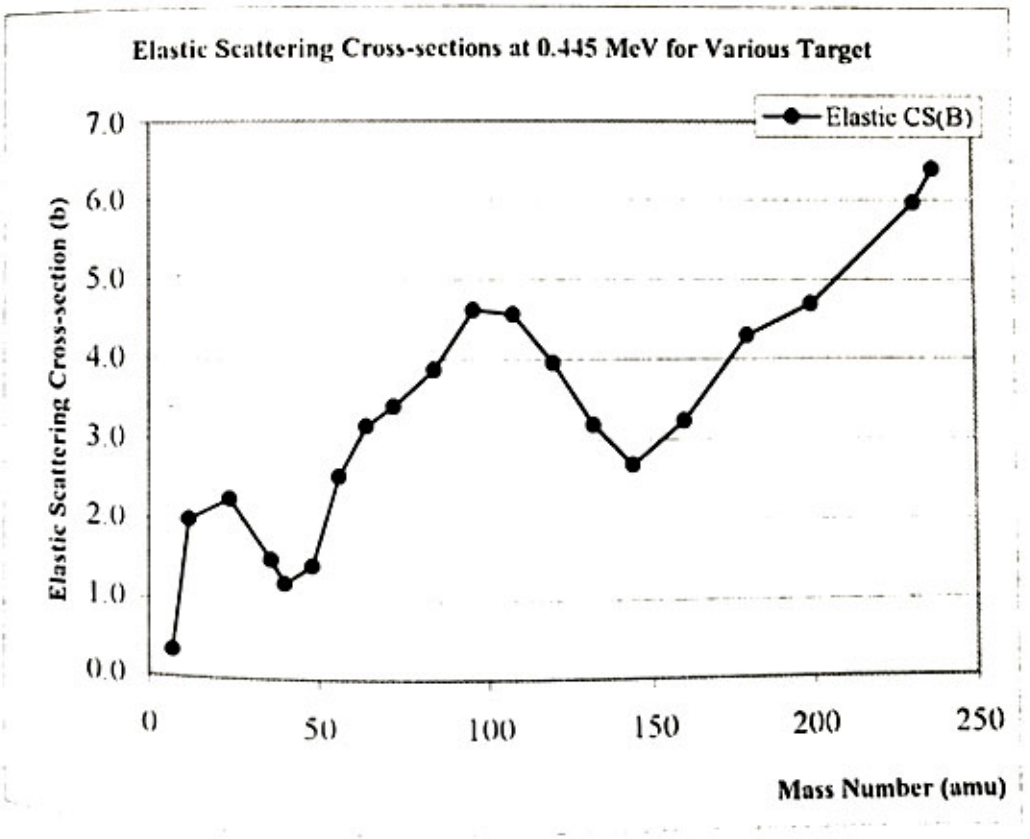

Fig (4.22) Elastic Scattering CS dependance of Mass Number at 0.445 MeV

Table (4.23) **Elastic Scattering CS at 0.485 MeV for Various Targets**

Target	A (amu)	Elastic CS(B)
3-Li	7	0.3375
6-C	12	1.9157
12-Mg	24	2.2662
17-Cl	36	1.5386
20-Ca	40	1.2276
22-Ti	48	1.3957
26-Fe	56	2.4230
30-Zn	64	3.0307
32-Ge	72	3.2810
38-Sr	84	3.7928
42-Mo	96	4.5887
48-Cd	108	4.5779
50-Sn	120	3.9983
54-Xe	132	3.2409
60-Nd	144	2.7318
64-Gd	160	3.1724
72-Hf	180	4.1056
81-Tl	200	4.4662
90-Th	232	5.7738
92-U	238	6.2156

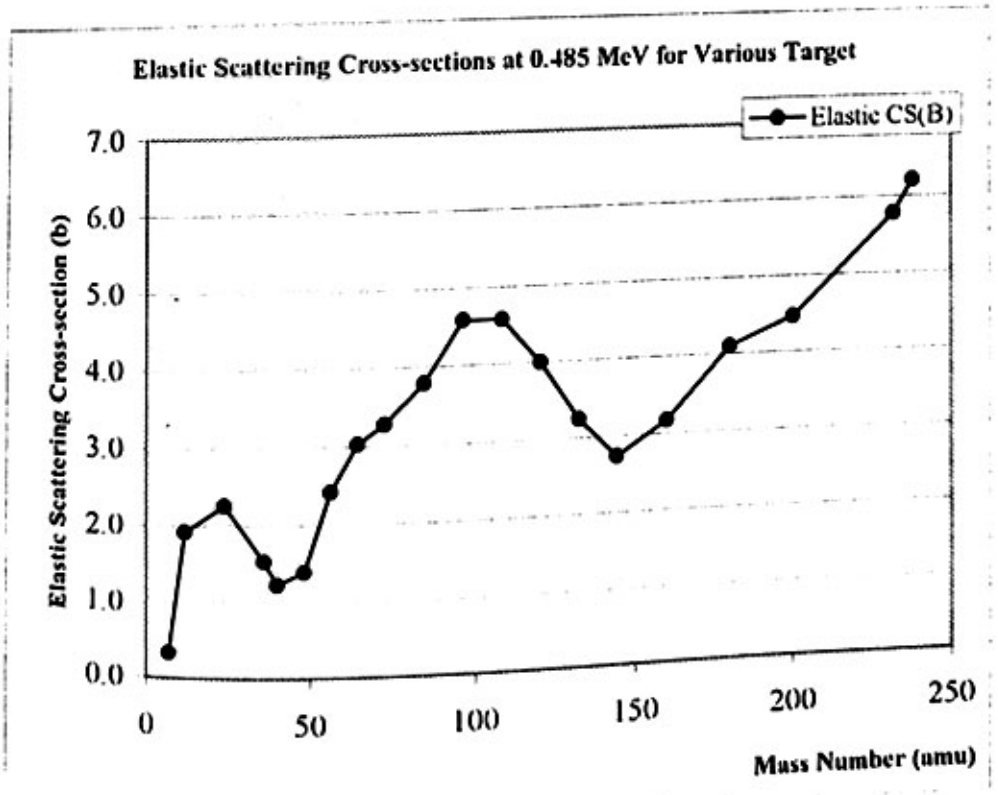

Fig (4.23) Elastic Scattering CS dependance of Mass Number at 0.485 MeV

Table (4.24) Elastic Scattering CS at 1 MeV for Various Targets

Target	A (amu)	Elastic CS(B)
3-Li	7	0.3356
6-C	12	1.2212
12-Mg	24	2.2438
17-Cl	36	1.7847
20-Ca	40	1.4807
22-Ti	48	1.2947
26-Fe	56	1.6268
30-Zn	64	1.9143
32-Ge	72	2.1180
38-Sr	84	2.8434
42-Mo	96	3.8970
48-Cd	108	4.2793
50-Sn	120	4.1112
54-Xe	132	3.7552
60-Nd	144	3.4969
64-Gd	160	3.3920
72-Hf	180	3.2745
81-Tl	200	3.3081
90-Th	232	3.8815
92-U	238	4.2494

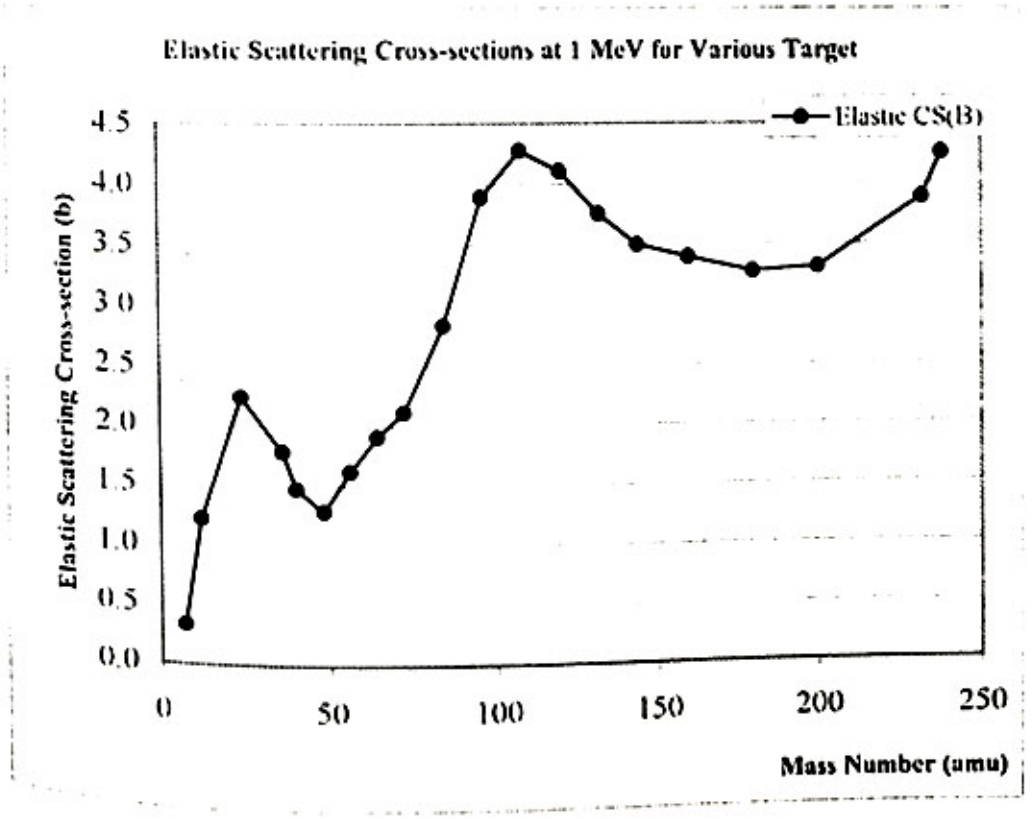

Fig (4.24) Elastic Scattering CS dependance of Mass Number at 1 MeV

Table (4.25) Elastic Scattering CS at 2 MeV for Various Targets

Target	A (amu)	Elastic CS(B)
3-Li	7	0.4035
6-C	12	0.6988
12-Mg	24	1.8889
17-Cl	36	1.9903
20-Ca	40	1.894
22-Ti	48	1.748
26-Fe	56	1.6194
30-Zn	64	1.4773
32-Ge	72	1.4076
38-Sr	84	1.7851
42-Mo	96	2.5224
48-Cd	108	3.0554
50-Sn	120	3.3868
54-Xe	132	3.7427
60-Nd	144	4.0725
64-Gd	160	4.1541
72-Hf	180	3.7748
81-Tl	200	3.3013
90-Th	232	3.1458
92-U	238	3.2071

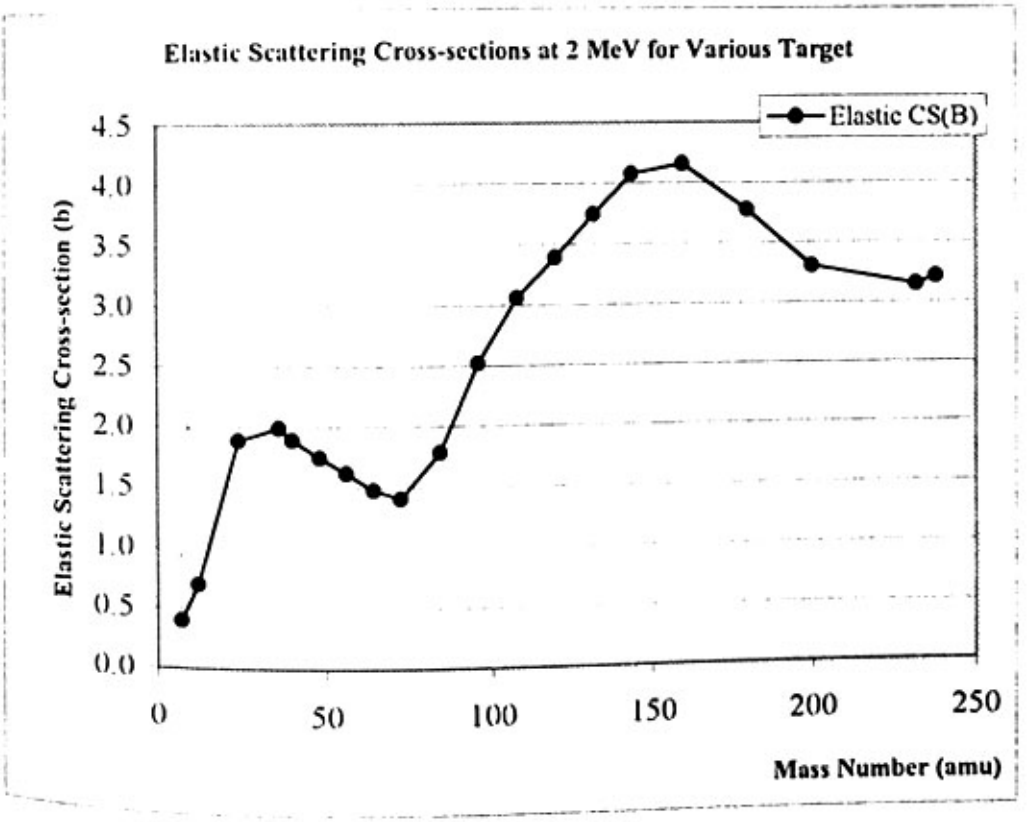

Fig (4.25) Elastic Scattering CS dependance of Mass Number at 2 MeV

Table (4.26) **Elastic Scattering CS at 3 MeV for Various Targets**

Target	A (amu)	Elastic CS(B)
3-Li	7	0 4847
6-C	12	0 5307
12-Mg	24	1.4965
17-Cl	36	1.994
20-Ca	40	2.0729
22-Ti	48	2.068
26-Fe	56	1 884
30-Zn	64	1 6489
32-Ge	72	1.4946
38-Sr	84	1.5409
42-Mo	96	1.8497
48-Cd	108	2.1744
50-Sn	120	2.5543
54-Xe	132	3.0753
60-Nd	144	3.59
64-Gd	160	3.9776
72-Hf	180	4.0649
81-Tl	200	4.0363
90-Th	232	3.7322
92-U	238	3.6638

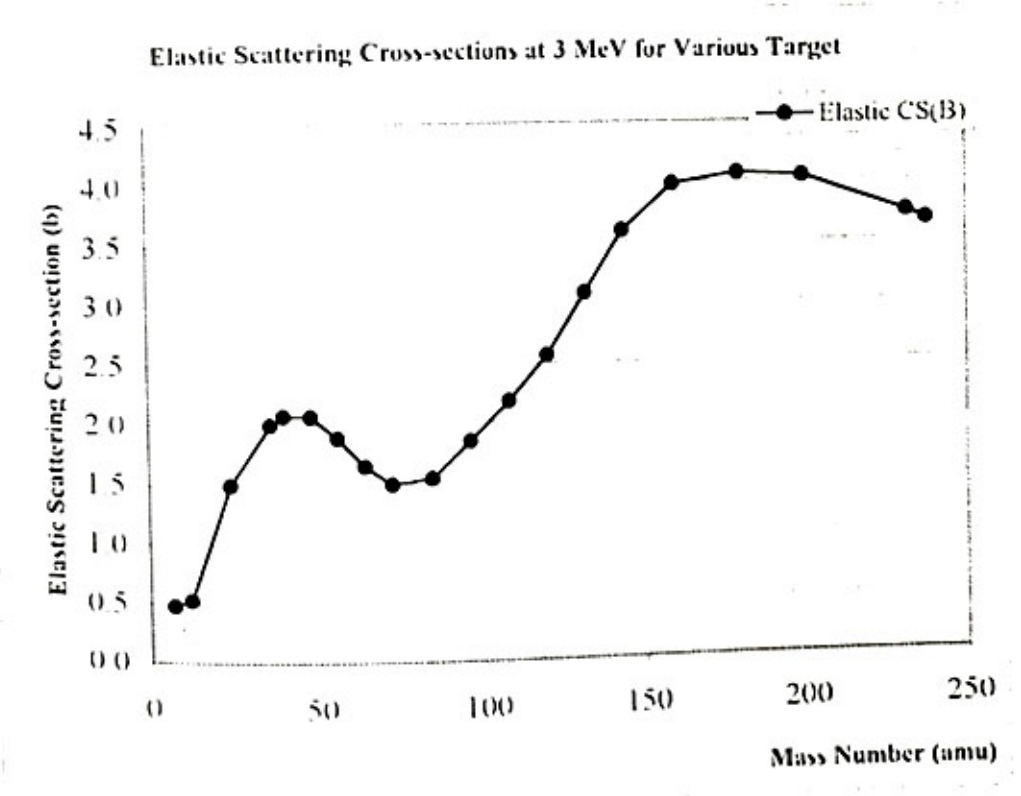

Fig (4.26) Elastic Scattering CS dependance of Mass Number at 3 MeV

Table (4.27) **Elastic Scattering CS at 4 MeV for Various Targets**

Target	A (amu)	Elastic CS(B)
3-Li	7	0.5708
6-C	12	0.4915
12-Mg	24	1.1853
17-Cl	36	1.8677
20-Ca	40	2.0336
22-Ti	48	2.1609
26-Fe	56	2.0777
30-Zn	64	1.938
32-Ge	72	1.8046
38-Sr	84	1.659
42-Mo	96	1.6652
48-Cd	108	1.777
50-Sn	120	2.0367
54-Xe	132	2.4518
60-Nd	144	2.9216
64-Gd	160	3.4123
72-Hf	180	3.8612
81-Tl	200	4.2022
90-Th	232	4.2018
92-U	238	4.1524

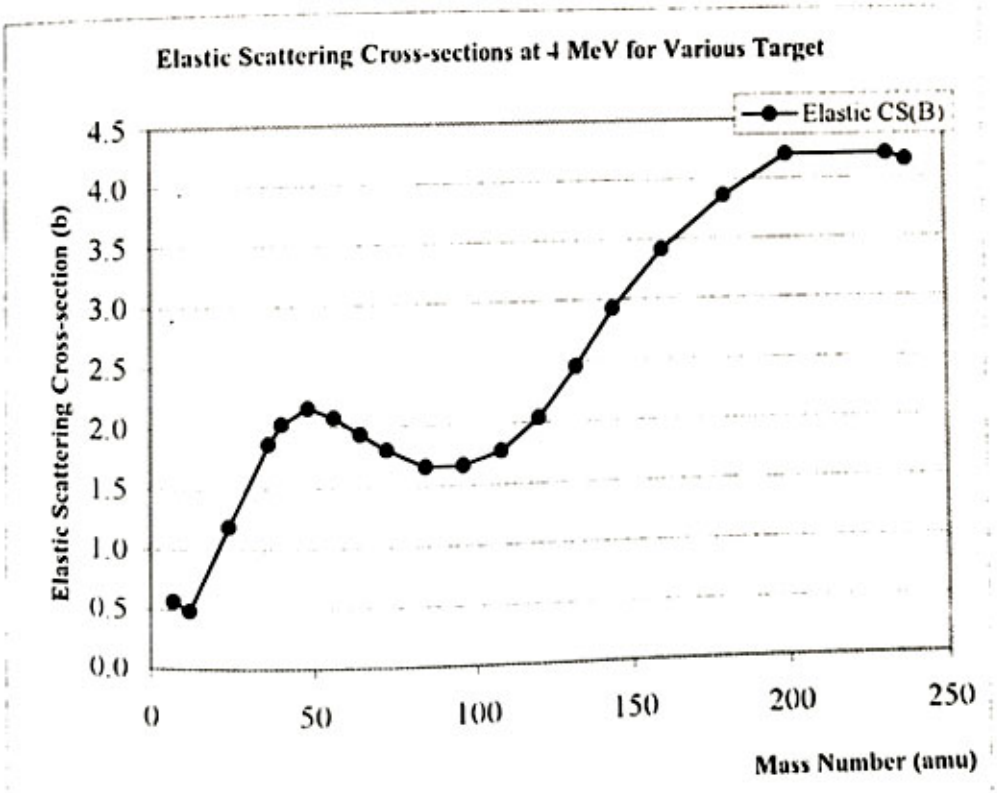

Fig (4.27) Elastic Scattering CS dependance of Mass Number at 4 MeV

Table (4.28) Elastic Scattering CS at 5 MeV for Various Targets

Target	A (amu)	Elastic CS(B)
3-Li	7	0.6519
6-C	12	0.5045
12-Mg	24	0.9605
17-Cl	36	1.6795
20-Ca	40	1.8835
22-Ti	48	2.1169
26-Fe	56	2.1755
30-Zn	64	2.1641
32-Ge	72	2.0759
38-Sr	84	1.8782
42-Mo	96	1.7545
48-Cd	108	1.742
50-Sn	120	1.8309
54-Xe	132	2.0677
60-Nd	144	3.3967
64-Gd	160	2.8452
72-Hf	180	3.4161
81-Tl	200	3.9431
90-Th	232	4.3108
92-U	238	4.3314

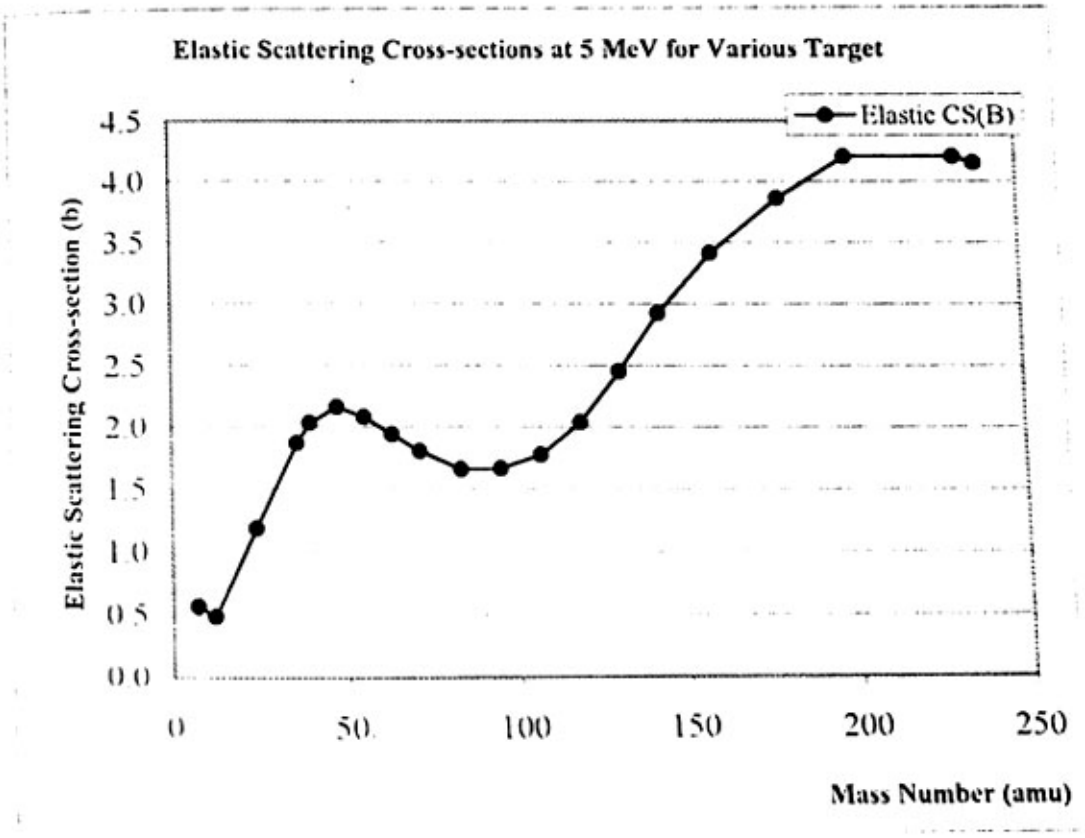

Fig (4.28) Elastic Scattering CS dependance of Mass Number at 5 MeV

Table (4.29) Elastic Scattering CS at 6 MeV for Various Targets

Target	A (amu)	Elastic CS(B)
3-Li	7	0.7177
6-C	12	0.5407
12-Mg	24	0.8073
17-Cl	36	1.4802
20-Ca	40	1.6945
22-Ti	48	2.0015
26-Fe	56	2.1824
30-Zn	64	2.2745
32-Ge	72	2.2508
38-Sr	84	2.1001
42-Mo	96	1.9731
48-Cd	108	1.8815
50-Sn	120	1.8311
54-Xe	132	1.9116
60-Nd	144	2.1024
64-Gd	160	2.4436
72-Hf	180	2.9486
81-Tl	200	3.5102
90-Th	232	4.1330
92-U	238	4.2144

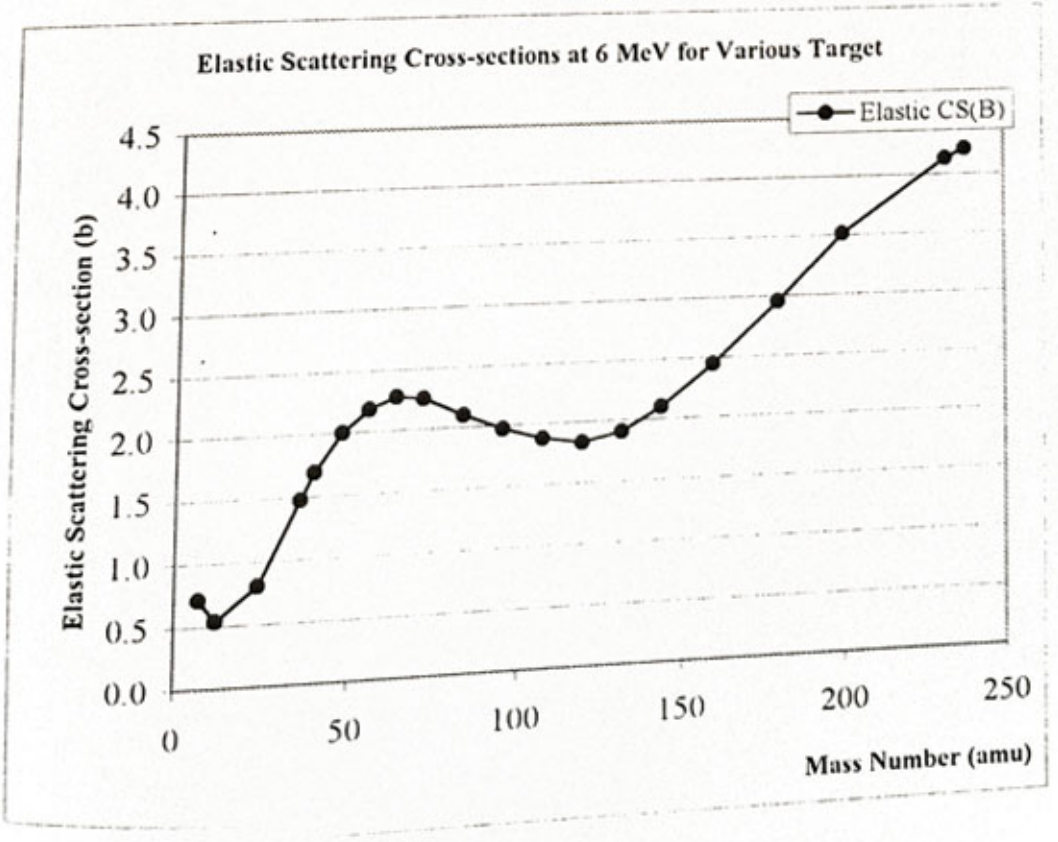

Fig (4.29) Elastic Scattering CS dependance of Mass Number at 6 MeV

Table (4.30) Elastic Scattering CS at 7 MeV for Various Targets

Target	A (amu)	Elastic CS(B)
3-Li	7	0.7658
6-C	12	0.5896
12-Mg	24	0.7095
17-Cl	36	1.2960
20-Ca	40	1.5038
22-Ti	48	1.8532
26-Fe	56	2.1172
30-Zn	64	2.2858
32-Ge	72	2.3349
38-Sr	84	2.2824
42-Mo	96	2.2056
48-Cd	108	2.0761
50-Sn	120	1.9528
54-Xe	132	1.9362
60-Nd	144	2.0255
64-Gd	160	2.2142
72-Hf	180	2.5753
81-Tl	200	3.0798
90-Th	232	3.7985
92-U	238	3.9100

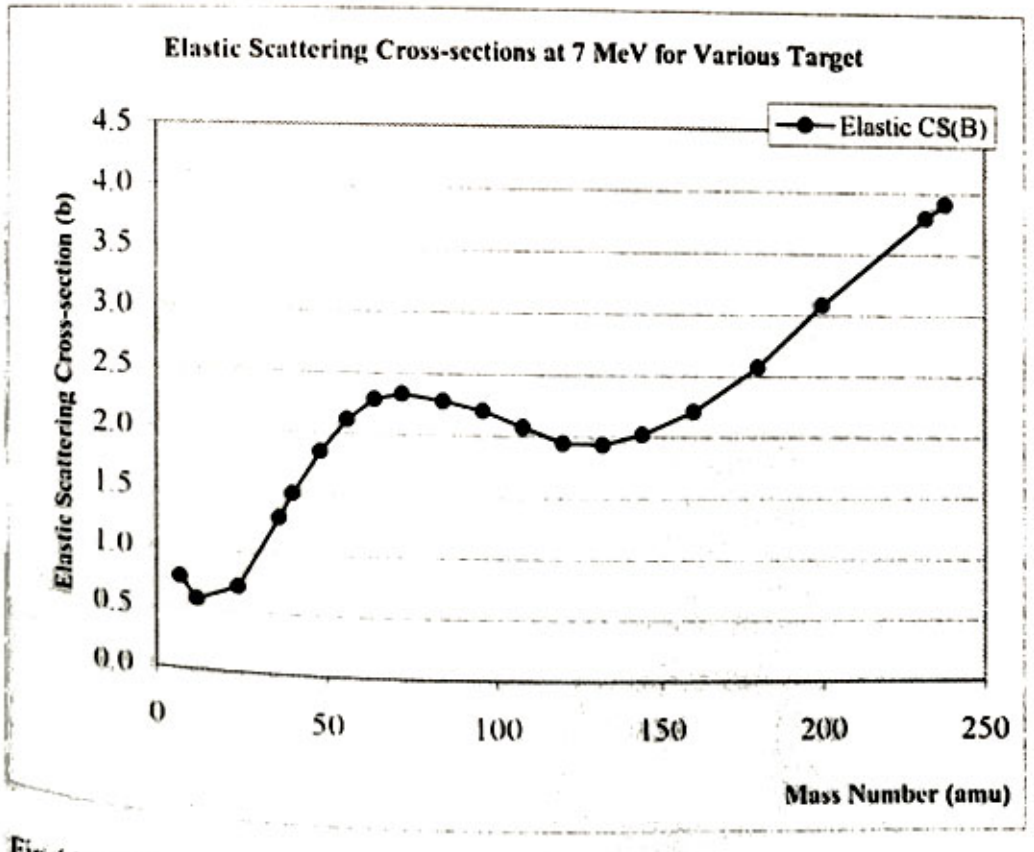

Fig (4.30) Elastic Scattering CS dependance of Mass Number at 7 MeV

Table (4.31) Elastic Scattering CS at 8 MeV for Various Targets

Target	A (amu)	Elastic CS(B)
3-Li	7	0.7987
6-C	12	0.6455
12-Mg	24	0.6545
17-Cl	36	1.1375
20-Ca	40	1.3299
22-Ti	48	1.6949
26-Fe	56	2.0046
30-Zn	64	2.2271
32-Ge	72	2.3465
38-Sr	84	2.4097
42-Mo	96	2.3924
48-Cd	108	2.2721
50-Sn	120	2.1373
54-Xe	132	2.0809
60-Nd	144	2.0895
64-Gd	160	2.1286
72-Hf	180	2.3436
81-Tl	200	2.7536
90-Th	232	3.4123
92-U	238	3.5309

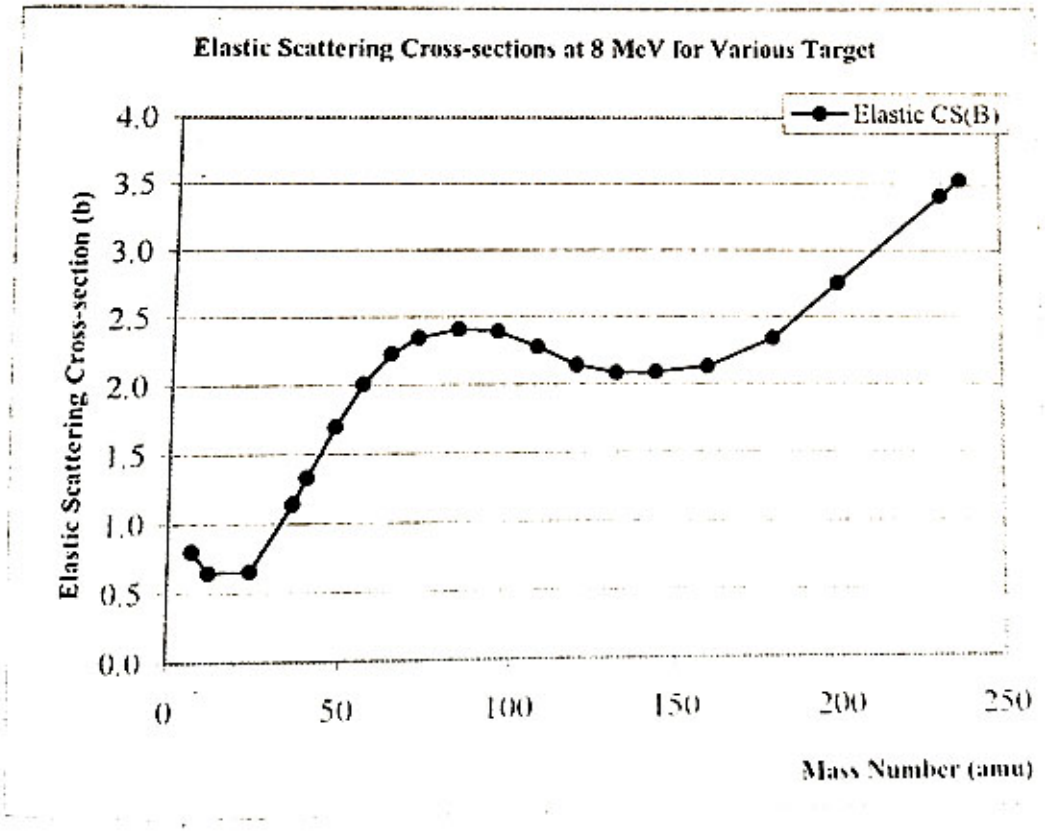

Fig (4.31) Elastic Scattering CS dependance of Mass Number at 8 MeV

Table (4.32) Elastic Scattering CS at 9 MeV for Various Targets

Target	A (amu)	Elastic CS(B)
3-Li	7	0.8203
6-C	12	0.7031
12-Mg	24	0.6330
17-Cl	36	1.0083
20-Ca	40	1.1816
22-Ti	48	1.5406
26-Fe	56	1.8663
30-Zn	64	2.1243
32-Ge	72	2.3044
38-Sr	84	2.4698
42-Mo	96	2.5176
48-Cd	108	2.4431
50-Sn	120	2.3408
54-Xe	132	2.2771
60-Nd	144	2.2238
64-Gd	160	2.1596
72-Hf	180	2.2603
81-Tl	200	2.5488
90-Th	232	3.0604
92-U	238	3.1723

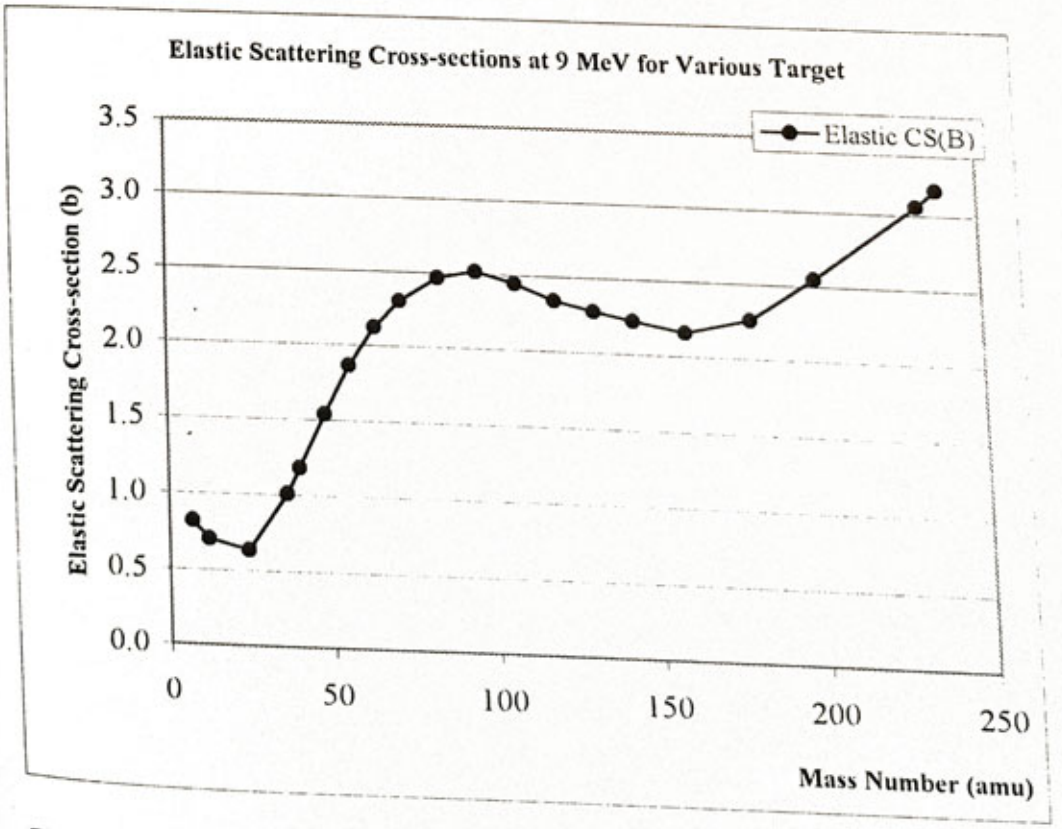

Fig (4.32) Elastic Scattering CS dependance of Mass Number at 9 MeV

Table (4.33) Elastic Scattering CS at 10 MeV for Various Targets

Target	A (amu)	Elastic CS(B)
3-Li	7	0.8342
6-C	12	0.7573
12-Mg	24	0.6367
17-Cl	36	0.909
20-Ca	40	1.0618
22-Ti	48	1.3984
26-Fe	56	1.7181
30-Zn	64	1.9973
32-Ge	72	2.2248
38-Sr	84	2.4702
42-Mo	96	2.5829
48-Cd	108	2.5759
50-Sn	120	2.5287
54-Xe	132	2.4744
60-Nd	144	2.3896
64-Gd	160	2.2762
72-Hf	180	2.2972
81-Tl	200	2.4471
90-Th	232	2.7989
92-U	238	2.8964

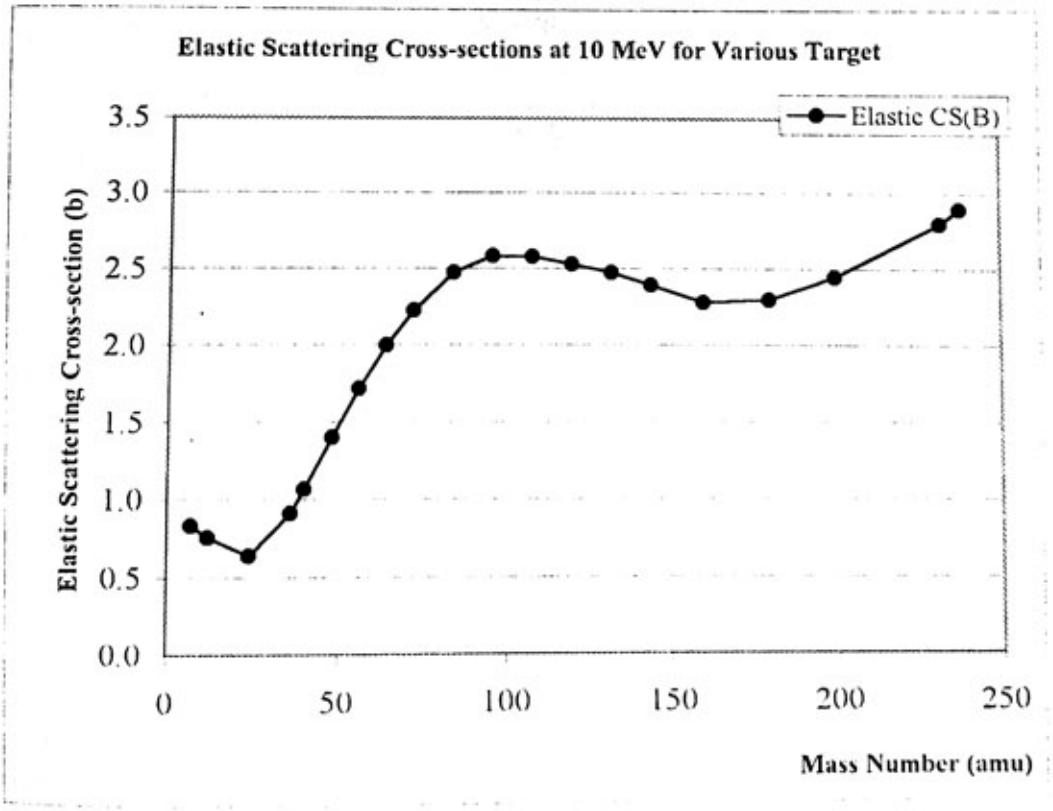

Fig (4.33) Elastic Scattering CS dependance of Mass Number at 10 MeV

Table (4.34) The Elastic Cross-section of 12-Mg-24

E (MeV)	Scat2_Cs(b)	Jendle_CS(b)	Error(%)
1.0000	2.2437	3.4153	-52.22
2.0000	1.8889	2.2751	-20.45
3.0000	1.4965	1.6653	-11.28
4.0000	1.1853	1.4029	-18.36
5.0000	0.9605	1.1458	-19.29
6.0000	0.8073	0.9562	-18.44
7.0000	0.7095	0.7966	-12.28
8.0000	0.6545	0.6991	-6.81
9.0000	0.6329	0.6402	-1.15
10.0000	0.6367	0.6209	2.48

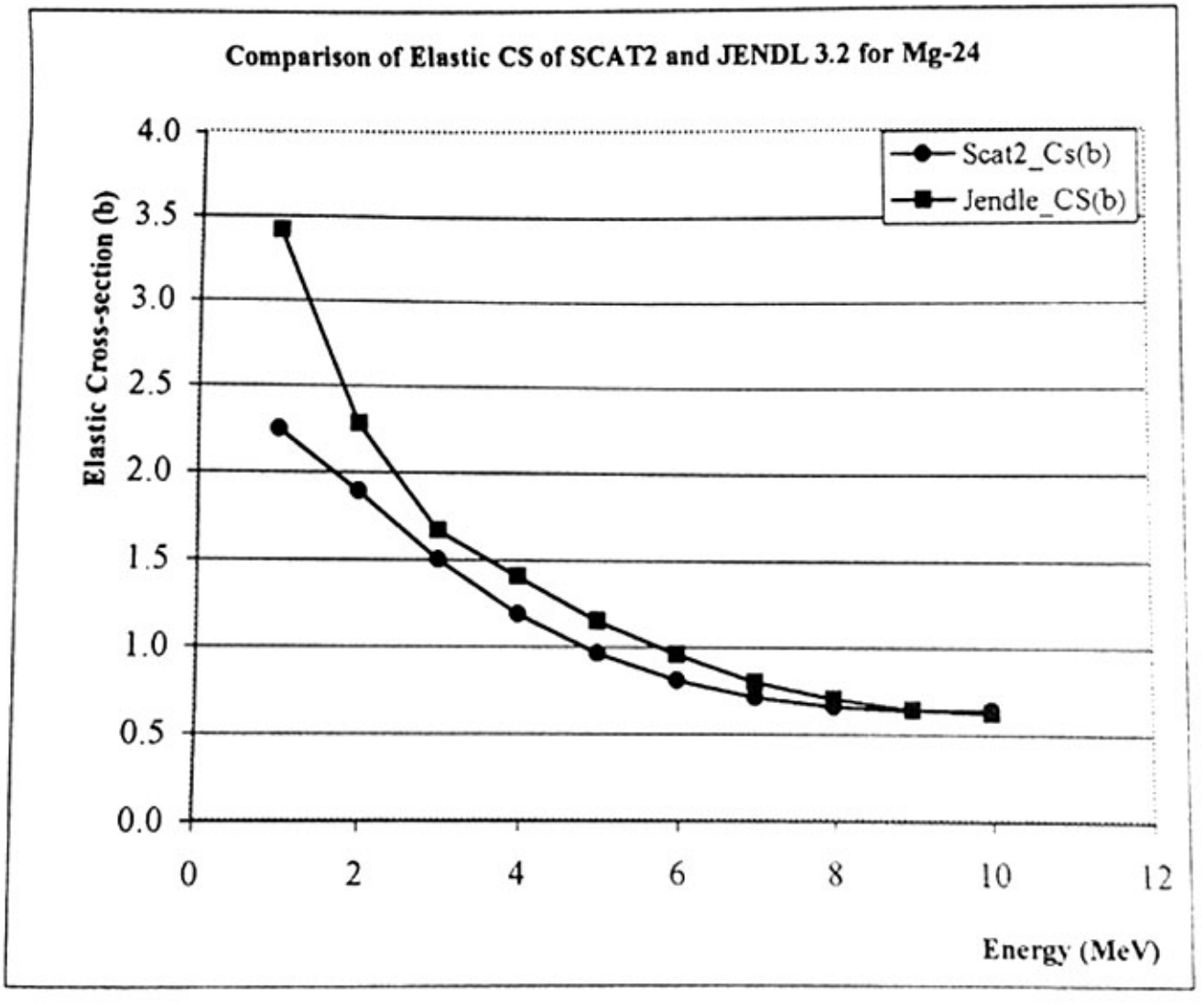

Fig (4.34) Comparison of Elastic CS of SCAT2 and JENDL 3.2 for 12-Mg-24

Table (4.35) The Elastic Cross-section of 92-U-238

E (MeV)	Scat2_Cs(b)	Jendle_CS(b)	Error(%)
1.0	4.2494	4.5372	-6.77
2.0	3.2071	3.5961	-12.13
3.0	3.6638	4.0847	-11.49
4.0	4.1524	4.3800	-5.48
5.0	4.3314	4.2500	1.88
6.0	4.2144	3.8687	8.2
7.0	3.9100	3.4274	12.34
8.0	3.5309	3.0472	13.7
9.0	3.1723	2.7737	12.57
10.0	2.8974	2.6105	9.9

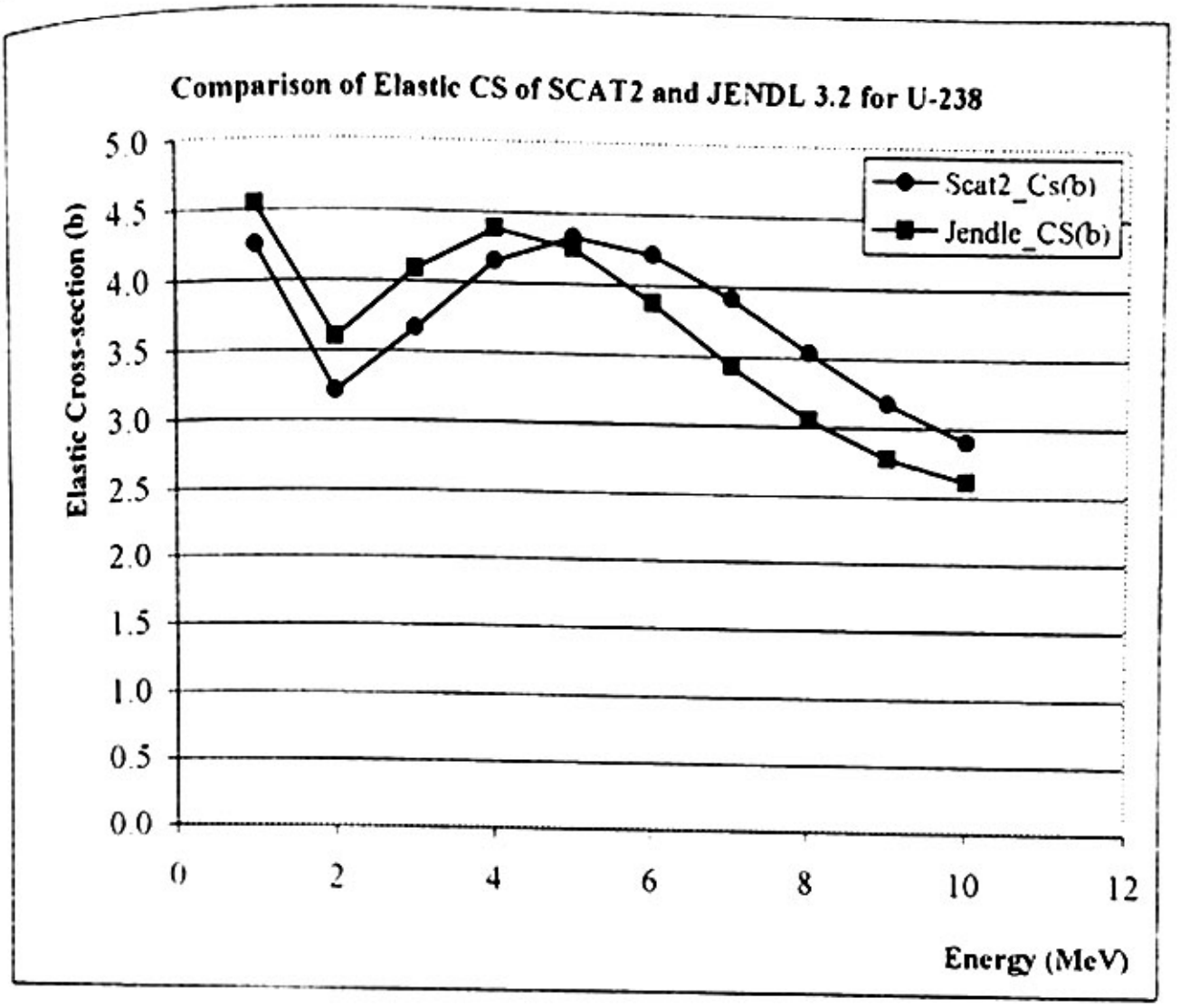

Fig (4.35) Comparison of Elastic CS of SCAT2 and JENDL 3.2 for 92-U-238

4.5 Conclusion

It is found that the dependence of total cross-sections of mass number shows the characteristics of peaks at mass number 6, 50 and 150. But the agreement is more obviously in high energy range. At high energy level it increases with increasing mass number. We can say that elastic scattering cross-sections depend on target mass number.

REFERENCES

1 Aung Kyi Myint 2004 "Optical Model Parameter Generator" PhD Thesis Yangon University

2 Aye Myat Mynn "Calculation And Analysis of Neutron Cross-Sections Using IAEA Nuclear Code SCAT2 With Different Energy Ranges" PhD Thesis, Yangon University

3 Enge H A 1975 "Introduction to Nuclear Physics" (London: Addison-Wesley)

4 ICTP 1984 "Nuclear Theory for Applications – 1982" (Vienna: IAEA)

5 Jackson D F 1970 "Nuclear Reactions" (London: Methuen)

6 Kaplan I 1962 "Nuclear Physics" (New York: Addison–Wesley)

7 Morrison P & Feld B T 1953 "Experimental Nuclear Physics" (London: Chapman & Hall)

8 Myint Myint Moe 2002 "Calculations and Analyses of Neutron Cross Sections Using IAEA Nuclear Code ABAREX with Different Energy Ranges" PhD Thesis Yangon University

9 Oliver Bersillon 1984 "SCAT2:UN PROGRAMME DE MODELE OPTIQUE SPHERIQUE" (Centre d'Dtudes de Bruyeres-le-Chatel)

10 Rightmyer Kennard & Lauritsen 1955 "Introduction to Modern Physics"

11 Sedre E 1953 "Experimental Nuclear Physics" (New York: John Wiley)

12 Stephenson R 1954 "Introduction to Nuclear Engineering" (London: McGraw-Hill)

13 The Web site http://www.t2lanl.gov "Nuclear Information Service, 12.1.2005"

14 Weisskopf B 1952 "Theoretical Nuclear Physics" (New York: John Wiley)